The Astronomical Journal, 129:809–828, 2005 February

B STAR ROTATIONAL VELOCITIES IN h AND χ PERSEI: A PROBE OF INITIAL CONDITIONS DURING THE STAR FORMATION EPOCH?

Stephen E. Strom[1] and Sidney C. Wolff[1]
National Optical Astronomy Observatory, P.O. Box 26732, Tucson, AZ 85726; sstrom@noao.edu

and

David H. A. Dror[1]
Cornell University, Ithaca, NY; and National Optical Astronomy Observatory, P.O. Box 26732, Tucson, AZ 85726
Received 2004 July 8; accepted 2004 October 13

ABSTRACT

Projected rotational velocities ($v \sin i$) have been measured for 216 B0–B9 stars in the rich, dense h and χ Persei double cluster and compared with the distribution of rotational velocities for a sample of field stars having comparable ages ($t \sim 12$–15 Myr) and masses ($M \sim 4$–15 $M_\odot$). For stars that are relatively little evolved from their initial locations on the zero-age main sequence (ZAMS) (those with masses $M \sim 4$–5 $M_\odot$), the mean $v \sin i$ measured for the h and χ Per sample is slightly more than 2 times larger than the mean determined for field stars of comparable mass, and the cluster and field $v \sin i$ distributions differ with a high degree of significance. For somewhat more evolved stars with masses in the range 5–9 $M_\odot$, the mean $v \sin i$ in h and χ Per is 1.5 times that of the field; the $v \sin i$ distributions differ as well, but with a lower degree of statistical significance. For stars that have evolved significantly from the ZAMS and are approaching the hydrogen exhaustion phase (those with masses in the range 9–15 $M_\odot$), the cluster and field star means and distributions are only slightly different. We argue that both the higher rotation rates and the pattern of rotation speeds as a function of mass that differentiate main-sequence B stars in h and χ Per from their field analogs were likely imprinted during the star formation process rather than a result of angular momentum evolution over the 12–15 Myr cluster lifetime. We speculate that these differences may reflect the effects of the higher accretion rates that theory suggests are characteristic of regions that give birth to dense clusters, namely, (1) higher initial rotation speeds; (2) higher initial radii along the stellar birth line, resulting in greater spin-up between the birth line and the ZAMS; and (3) a more pronounced maximum in the birth line radius-mass relationship that results in differentially greater spin-up for stars that become mid- to late-B stars on the ZAMS.

Key words: open clusters and associations: individual (NGC 869, NGC 884) — stars: formation — stars: rotation

1. INTRODUCTION

Much of our current understanding of how stars form derives from the study of nearby star-forming regions such as Taurus-Auriga, Ophiuchus, and Chamaeleon. These regions are populated by ~100 young stars having typical masses $M < 1$ $M_\odot$ contained within irregular molecular cloud complexes that span regions of size ~3–10 pc. However, the demographics and morphologies of these complexes differ markedly from those thought to produce the majority of stars over the history of the universe: dense stellar clusters containing 10^4–10^6 stars having masses ranging from 100 to 0.1 $M_\odot$ formed within regions no more than ~1 pc in size. Do the dramatic differences in stellar density between these regions influence measurable properties of individual stars and the statistical properties (e.g., the initial mass function [IMF]) of the emerging stellar populations? If so, what are the key physical causes? Answering these questions represents an essential first step toward developing a predictive theory of star formation of sufficient power to inform our understanding of how the mix of high- and low-mass stars populating galaxies today came to be and, as a consequence, how the observed relative abundances of heavy elements were established.

The importance and timeliness of these questions have stimulated several recent theoretical studies aimed at predicting initial protostellar conditions in dense star-forming complexes (e.g., McKee & Tan 2003) and their relationship to emergent stellar mass functions (e.g., Elmegreen & Shadmehri 2003). Dense stellar clusters form in regions of very high gas surface density, which are characterized as well by close packing of protostars. The turbulent velocity of the gas in these regions is likely to be high, leading to (1) protostars of high initial density, (2) rapid protostellar collapse times, and (3) as a consequence, high time-averaged accretion rates. The latter may be conducive to the formation of very high mass stars, since the dynamical pressure of accreting material can be high enough to overcome radiation pressure from the forming massive stars (McKee & Tan 2003). The combination of protostellar cores characterized by higher turbulent speeds and higher mass accretion rates, combined with collisions between closely packed cores, may in turn produce a "top-heavy" IMF (Elmegreen & Shadmehri 2003).

These theoretical studies thus suggest (1) higher time-averaged accretion rates and (2) an IMF biased toward higher mass stars in high-density stellar clusters. In principle, accretion rates characteristic of different star-forming regions can be diagnosed from the location of the stellar birth line (e.g., Stahler 1988) as determined from spectroscopic and photometric observations of precision sufficient to locate pre–main-sequence stars spanning a

[1] The National Optical Astronomy Observatory is operated by the Association of Universities for Research in Astronomy, Inc., under cooperative agreement with the National Science Foundation.

range of masses in the H-R diagram, provided that the target regions are young and accurate age estimates are available. Quantifying IMFs requires similar observations.

To date, it has not been possible to determine either birth line locations or IMFs spanning the full range of stellar masses, primarily because the best and closest examples of high-density clusters (e.g., Arches at the Galactic center, Stolte et al. 2002; R136 in the Magellanic Clouds, Massey & Hunter 1998; Sirianni et al. 2000) suffer from extreme crowding, which thus far has limited photometric and spectroscopic observations to main-sequence stars and a few pre–main-sequence stars with masses above $\sim$2 $M_{\odot}$. Such stars are both bright enough to stand out relative to the stellar background and rare enough to avoid overlap with objects of comparable brightness. Next-generation adaptive optics systems on current-generation large telescopes have the potential to overcome the limitations of crowding and enable determination of stellar luminosities and effective temperatures for stars with masses as small as 0.1 $M_{\odot}$, a level more than sufficient to confront theoretical predictions of IMF shape and birth line positions. However, until such systems become operational, other and less direct approaches must suffice. We explore here the possibility that the distribution of stellar rotational velocities can provide a surrogate indicator of the differences in initial conditions between low- and high-density star-forming regions. Our reasoning is as follows.

Current theory suggests that initial stellar angular momenta are established during the primary stellar accretion phase via locking of stellar angular velocity to the angular velocity of the circumstellar accretion disk at or near the radius, $r(m)$, where the stellar magnetosphere links to the disk (e.g., Königl 1991; Shu et al. 1994). That radius is set by the balance between the dynamical pressure of accreting material and the magnetic pressure of the magnetic field rooted in the forming star. For a fixed stellar magnetic field strength, the higher the accretion rate through the disk, the smaller the $r(m)$, the higher the Keplerian rotation speed of the disk at $r(m)$, and hence the higher the angular rotational speed of the star. Hence, if accretion rates are higher in high-density star-forming regions, the resulting stellar population would be expected to exhibit higher rotation speeds on average.

Supporting observational evidence in the literature is sparse but highly suggestive. For example, Wolff et al. (1982, hereafter WEP82) note that the distribution of rotation speeds among B stars in the relatively dense Orion Nebula Cluster is significantly shifted toward higher values as compared with stars of similar type distributed among the much lower density regions of the Orion star-forming complex. Similarly, Slettebak (1968) argues that stellar rotation speeds among the luminous B giant stars located in the vicinity of the extremely dense h and χ Per double cluster are $\sim$50% higher than their field counterparts. Moreover, he reports an unusually high number of rapidly rotating Be stars, possibly indicative of a higher fraction of rapidly rotating stars in h and χ Per. However, the Orion study includes only a modest sample of stars, whereas past discussions of h and χ Per rotation properties suffer from concerns regarding the similarity in age range among field and cluster cohorts combined with the possibility of evolutionary changes in stellar angular momenta. Confronting the hypothesis that stars born in dense clusters rotate more rapidly than their field counterparts requires sufficiently large samples of cluster and field stars spanning an identical range of ages.

The goal of this contribution is to effect a robust statistical comparison of the distribution of stellar rotational velocities for a sample of B0–B9 stars in h and χ Per (typical stellar density of 10^4 pc^{-3}; Slesnick et al. 2002, hereafter SHM02) with those observed among field B stars of comparable age as determined from their location in the Strömgren (β, c_0) plane. This latter sample is almost certainly dominated by stars born in much lower density environments.

2. NEW OBSERVATIONS OF B STARS IN h AND χ PER

2.1. *Spectroscopy*

We report here new rotational velocity determinations of 216 stars in h and χ Per with estimated masses greater than 4 $M_{\odot}$. These stars were chosen from the recent photometric and moderate-resolution spectroscopic study of the double cluster by SHM02. The basic data for the h and χ Per stars are listed in Table 1. Column (1) provides an identification from SHM02; column (2) lists the Oosterhoff number; columns (3) and (4) list, respectively, the absolute visual magnitude M_V and the log of the effective temperature derived by SHM02; column (5) lists the spectral type, if available; column (6) lists the mass derived by SHM02; column (7) lists the derived value of $v \sin i$ (see below); column (8) lists a group assigned to the star on the basis of its effective temperature (see below); in columns (9) and (10) we list the Strömgren indices c_0 and β, respectively, from the work of Capilla & Fabregat (2002) or Crawford et al. (1970); and in column (11), we indicate whether the star is judged to be a spectroscopic binary with velocity amplitude $K > 30$ km s^{-1} (see below). The H-R diagram for these stars is shown in Figure 1. Also shown are evolutionary tracks from Schaller et al. (1992), with the $M_{\rm bol}$ from these tracks converted to M_V by using the relationship between bolometric correction and $T_{\rm eff}$ given by SHM02.

For the purpose of later analysis, we divide the h and χ Per stars into three temperature groups, which are shown in Figure 1. We effected this division in order to examine separately the rotational properties of (1) relatively unevolved stars still located within 0.5 mag of the ZAMS, (2) stars located within 1 mag of the ZAMS, and (3) stars that have evolved significantly from the ZAMS. Comparison with the evolutionary tracks indicates that these three groups correspond to mass ranges of approximately 3.5–5, 5–9, and 9–15 $M_{\odot}$. These groups are identified in Table 1 (col. [8]) as group 1 (coolest and close to the ZAMS), group 2 (middle range of temperature and slightly evolved from the ZAMS), and group 3 (hottest and most evolved), respectively.

Spectra of the h and χ Per stars in our sample were obtained during three nights in 2002 September with the Hydra multifiber spectrograph and the WIYN 3.5 m telescope on Kitt Peak. The 316/63.4 echelle grating and a narrowband order-separating filter were used in conjunction with the red bench camera to produce spectra with resolution $\sim$0.2 Å centered at a wavelength of 4461 Å and spanning 120 Å. This wavelength region was selected in order to include the two strong features He I λ4471 and Mg II λ4481, which together provide the basis for determining accurate rotational velocities for stars in the desired spectral-type range, B0–B9.

Eight separate fiber settings enabled observations of a total of 216 stars. Three settings were targeted at the brighter members of the cluster ($8.5 < B < 12$) and five at the fainter members ($12 < B < 14.5$). Exposure times were 30–60 minutes (divided among three exposures) for the bright sample and 90–120 minutes (divided among three to four exposures) for the faint sample. The series of three exposures for the bright stars was repeated either one or two nights later. Flat-field exposures and wavelength-calibration observations derived from Th-Ar lamp spectra were obtained before or after each exposure.

TABLE 1

Data for Stars in h and χ Per

ID (1)	Oosterhoff (2)	M_V (3)	Log ($T_{\rm eff}$) (4)	Spectral Type (5)	Mass ($M_\odot$) (6)	$v \sin i$ (km s^{-1}) (7)	Group (8)	c_0 (9)	β (10)	Binarity (11)
9	2227	−5.57	4.375	B1.5 II	21	22	. . .	0.031	2.584	
12	662	−4.86	4.37	B1.5 I	16.4	22	3	0.007	2.582	
16	1132	−5.12	4.34	B2 I	16.8	60	. . .	. . .	. . .	
19	2296	−4.79	4.34	B2 I	15.1	146	. . .	0.05	2.598	
28	847	−4.47	4.37	B1.5 Ie	15.2	55	3	0.063	2.577	
32	2299	−4.05	4.37	B1.5 I	13.2	106	3	0.027	2.615	
33	2371	−4.44	4.355	B2 III	14	60	3	0.024	2.503	$\Delta v = -62$
36	2541	−4.4	4.36	B1.5 III	14.4	55	3	0.066	2.61	
40	1116	−4.65	4.45	B0.5 V	20	93	. . .	0.088	2.635	
41	2088	−4.41	4.372	B1 IIIe	14.8	89	3	0.01	2.506	
42	717	−4.09	4.405	B1 V	15	57	3	0.026	2.605	$\Delta v = 40$
43	843	−4.17	4.35	B1.5 V	13.2	88	3	0.091	2.589	
46	1268	−4.38	4.371	B0.5 V	14.6	127	3	0.032	2.579	
47	2311	−4.04	4.375	B1.5 II	13.3	20	3	0.065	2.602	
49	692	−3.81	4.44	B0.5 I	15.5	169	3	. . .	. . .	
52	782	−3.99	4.36	B1.5 III	12.7	36	3	0.095	2.53	
54	. . .	−4.01	4.361	. . .	12.9	116	3	. . .	. . .	
57	922	−4.15	4.397	B2 V	14.2	258	3	0.053	2.591	
58	1261	−4.72	4.502	B3 Ve	24	261	. . .	. . .	. . .	
66	2284	−4.24	4.484	Be	19.7	299	. . .	−0.082	2.381	
71	980	−3.82	4.355	B2 III	12	39	3	0.098	2.627	
72	1078	−3.81	4.405	B1 V	14.1	167	3	0.1	2.633	
77	. . .	−3.56	4.418	. . .	13.8	108	3	. . .	. . .	
78	1364	−3.66	4.322	. . .	11.1	203	2	. . .	. . .	
81	864	−3.57	4.328	B2 V	10.8	113	3	0.14	2.561	
83	2246	−3.47	4.355	B2 III	11.5	101	3	0.04	2.623	
87	517	−3.25	4.267	Be	8.8	178	. . .	. . .	. . .	
91	. . .	−3.58	4.358	. . .	11.3	264	3	. . .	. . .	
96	2165	−3.5	4.405	B1 Ve	13.2	79	3	0.047	2.494	
100	1161	−3.73	4.405	B1 Ve	13.8	135	3	0.045	2.588	
102	. . .	−3.11	4.349	. . .	10.6	58	3	. . .	. . .	
106	929	−3.39	4.36	B1.5 III	11.5	151	3	0.115	2.618	
109	. . .	−3.23	4.314	. . .	9.6	161	2	. . .	. . .	
117	936	−3.18	4.35	B1.5 V	10.8	26	3	0.063	2.622	
120	1085	−3.22	4.355	B2 III	10.9	59	3	0.062	2.641	
121	. . .	−3.22	4.347	. . .	10.8	20	3	. . .	. . .	
131	2262	−3.13	4.36	B1.5 III	10.9	204	3	0.124	2.574	
133	. . .	−3.05	4.389	. . .	11.6	248	3	. . .	. . .	
138	. . .	−2.9	4.32	. . .	9.5	115	2	. . .	. . .	
141	2566	−3.21	4.334	Be	10.4	183	3	. . .	. . .	$\Delta v = -44$
144	978	−2.99	4.33	B2 IV	9.8	29	3	0.085	2.625	
149	. . .	−2.9	4.332	. . .	9.8	77	3	. . .	. . .	
150	. . .	−2.67	4.363	. . .	10.1	22	3	. . .	. . .	
158	859	−2.85	4.3	B2 V	9	192	2	0.168	2.578	
160	. . .	−2.88	4.294	. . .	9	156	2	. . .	. . .	
163	. . .	−2.93	4.319	. . .	9.5	20	2	. . .	. . .	
165	. . .	−2.68	4.345	. . .	9.7	60	3	. . .	. . .	
171	622	−2.34	4.355	B2 III	9.4	57	3	. . .	. . .	
177	. . .	−2.53	4.347	. . .	9.5	77	3	. . .	. . .	
178	2185	−2.59	4.33	B2 IV	9.2	155	3	0.326	2.7	
184	. . .	−3	4.357	. . .	10.6	48	3	. . .	. . .	
188	. . .	−2.42	4.316	. . .	8.6	33	2	. . .	. . .	
189	1282	−2.58	4.38	Be	10.4	264	3	0.037	2.509	
191	1109	−2.77	4.3	B2 V	8.9	170	2	0.174	2.67	
193	919	−2.97	4.294	. . .	8.5	94	2	. . .	. . .	
194	. . .	−2.08	4.218	B5 II	6.7	67	. . .	. . .	. . .	
198	. . .	−2.7	4.295	. . .	8.7	57	2	. . .	. . .	
200	963	−2.26	4.3	B2.5 II	8.1	29	2	0.114	2.651	
201	. . .	−2.53	4.324	. . .	9	72	2	. . .	. . .	
202	2114	−2.48	4.3	B2 V	8.4	169	2	. . .	. . .	
203	2232	−2.15	4.27	B3 V	7.5	101	2	0.127	2.651	
205	. . .	−2.35	4.293	. . .	8.1	215	2	. . .	. . .	
206	. . .	−2.17	4.293	. . .	7.9	209	2	. . .	. . .	
208	1041	−2.51	4.3	B2 V	8.5	154	2	0.151	2.668	

TABLE 1—*Continued*

ID (1)	Oosterhoff (2)	M_V (3)	Log ($T_{\rm eff}$) (4)	Spectral Type (5)	Mass ($M_{\odot}$) (6)	$v \sin i$ (km s^{-1}) (7)	Group (8)	c_0 (9)	β (10)	Binarity (11)
219	892	−2.24	4.29	B2.5 III	7.9	61	2	0.136	2.63	
222	...	−2.44	4.313	...	8.6	31	2	...	...	
223	...	−2.21	4.335	...	8.8	238	3	...	...	
231	...	−2.62	4.344	...	9.5	51	3	...	...	
235	950	−2.36	4.33	B2 IV	8.8	89	3	0.105	2.593	
237	...	−2.4	4.292	...	8.2	312	2	...	...	
239	2229	−2.16	4.27	B3 V	7.5	235	2	...	...	
240	...	−2.29	4.308	...	8.3	242	2	...	...	
241	...	−2.13	4.328	...	8.5	137	2	...	...	
265	...	−1.83	4.281	...	7.3	261	2	...	...	
277	...	−2.14	4.288	...	7.8	109	2	...	...	
280	...	−2.02	4.332	...	8.5	69	3	...	...	
284	...	−2.01	4.355	B2 III	9	68	3	...	...	
288	879	−1.97	4.3	B2 V	7.8	91	2	0.138	2.619	
289	...	−1.96	4.272	...	7.3	194	2	...	...	
297	...	−2.31	4.338	...	9	160	3	...	...	
298	...	−1.93	4.299	...	7.7	112	2	...	...	$\Delta v = -41$
299	...	−2.04	4.298	...	7.8	254	2	...	...	
314	2091	−2.06	4.288	Be	7.7	167	2	...	...	
315	...	−1.89	4.267	...	7.1	239	2	...	...	
318	...	−1.85	4.244	...	6.8	110	2	...	...	
331	...	−1.71	4.235	...	6.5	42	2	...	...	SB2; $\Delta v = 106$
331	...	−1.71	4.235	...	6.5	20	2	...	...	SB2
338	...	−1.69	4.271	...	7	50	2	...	...	
341	...	−1.74	4.275	...	7.1	178	2	...	...	
350	...	−1.68	4.267	...	6.9	82	2	...	...	
359	2140	−1.7	4.19	B5 V	6	72	...	...	...	
362	...	−1.91	4.272	...	7.2	101	2	...	...	
363	...	−1.47	4.271	...	6.8	338	2	...	...	
369	2301	−1.58	4.3	B2 V	7.4	135	2	...	...	$\Delta v = 31$
393	778	−1.55	4.35	B1.5 V	8.4	225	...	0.293	2.571	
394	869	−1.45	4.3	B2 V	7.3	254	2	0.407	2.686	
401	952	−1.36	4.242	...	6.3	219	2	0.323	2.692	
404	...	−1.59	4.274	...	7	42	2	...	...	
409	...	−1.5	4.269	...	6.8	237	2	...	...	
415	...	−1.49	4.24	...	6.4	125	2	...	...	
431	...	−1.29	4.284	...	6.8	207	2	...	...	
436	2379	−1.3	4.3	B2 V	7.1	244	2	...	...	
439	800	−1.3	4.3	B2 V	7.2	234	2	0.298	2.588	
443	...	−1.6	4.275	...	7	28	2	...	...	SB2; $\Delta v = 111$
443	...	−1.6	4.275	...	7	20	2	...	...	SB2
444	...	−0.78	4.196	...	5.3	267	1	...	...	
450	...	−1.25	4.247	...	6.3	77	2	...	...	
452	2352	−1.22	4.23	B3 III	6	74	2	...	...	
453	...	−1.36	4.277	...	6.8	109	2	...	...	
460	...	−1.29	4.281	...	6.8	69	2	...	...	
494	...	−0.96	4.129	...	4.9	169	...	...	...	
497	...	−1.09	4.23	...	5.9	101	2	...	...	
500	...	−1.07	4.259	...	6.3	241	2	...	...	
501	...	−1.38	4.256	...	6.5	100	2	...	...	
506	...	−0.9	4.236	...	5.9	90	2	...	...	$\Delta v = -67$
507	...	−1.28	4.256	...	6.4	29	2	...	...	SB2; $\Delta v = 104$
507	...	−1.28	4.256	...	6.4	20	2	...	...	SB2
513	896	−1.17	4.35	B1.5 V	7.9	403	...	0.344	2.649	
514	...	−1.22	4.157	...	5.2	21	...	...	...	
517	...	−1.37	4.229	...	6.1	111	2	...	...	
520	956	−1.17	4.243	...	6.2	83	2	0.371	2.716	
531	...	−0.74	4.234	...	5.7	168	2	...	...	
533	...	−0.98	4.323	...	7.2	196	...	...	...	
537	...	−0.92	4.189	...	5.3	137	1	...	...	
540	965	−1.17	4.27	B3 V	6.5	82	2	0.329	2.669	
543	...	−0.74	4.184	...	5.1	20	1	...	...	SB2; $\Delta v = 126$
543	...	−0.74	4.184	...	5.1	20	1	...	...	SB2
549	...	−1.13	4.257	...	6.3	248	2	...	...	
551	...	−0.87	4.2	...	5.4	271	1	...	...	

TABLE 1—*Continued*

ID (1)	Oosterhoff (2)	M_V (3)	Log ($T_{\rm eff}$) (4)	Spectral Type (5)	Mass ($M_{\odot}$) (6)	$v \sin i$ (km s^{-1}) (7)	Group (8)	c_0 (9)	β (10)	Binarity (11)
554	...	−0.75	4.205	...	5.4	141	1	...	...	
562	...	−0.86	4.286	...	6.5	81	2	...	...	
565	...	−0.88	4.234	...	5.8	61	2	...	...	
576	876	−0.98	4.27	B3 V	6.4	115	2	0.327	2.665	
587	...	−0.94	4.223	...	5.7	306	2	...	...	
590	...	−0.5	4.179	...	4.9	53	1	...	...	
594	...	−0.62	4.229	...	5.6	85	2	...	...	
598	...	−0.46	4.161	...	4.7	215	1	...	...	
600	...	−0.65	4.212	...	5.4	32	1	...	...	
602	2349	−0.78	4.29	B2.5 V	6.5	261	2	0.43	2.68	
611	...	−0.5	4.116	...	4.4	237	...	...	...	
616	...	−0.9	4.262	...	6.2	254	2	...	...	
628	...	−0.86	4.223	...	5.7	58	2	...	...	
632	...	−0.85	4.211	...	5.5	248	1	...	...	
641	...	−0.64	4.219	...	5.5	299	1	...	...	
650	872	−0.89	4.3	B2 V	6.8	332	2	0.369	2.588	
655	2297	−0.47	4.19	B5 V	5	254	1	0.383	2.712	
658	2211	−0.49	4.27	B3 V	6	282	2	0.475	2.765	
670	...	−0.22	4.153	...	4.5	30	1	...	...	
675	659	−0.38	4.19	B5 V	5	153	1	...	...	
681	...	−0.47	4.167	...	4.8	239	1	...	...	
683	2345	−0.51	4.27	B3 V	6	108	2	0.415	2.742	
687	...	−0.76	4.241	...	5.8	203	2	...	...	
701	...	−0.33	4.206	...	5.1	67	1	...	...	
709	923	−0.21	4.203	...	5	38	1	0.37	2.723	
721	2275	−0.6	4.246	...	5.8	184	2	0.385	2.715	
726	...	−0.33	4.161	...	4.7	33	1	...	...	
736	1066	−0.6	4.2	...	5.2	153	1	0.458	2.716	
749	...	−0.38	4.214	...	5.2	251	1	...	...	
753	...	−0.21	4.123	...	4.3	207	...	...	...	
754	820	−0.23	4.164	B V	4.6	319	1	0.521	2.661	
765	...	−0.68	4.204	...	5.3	185	1	...	...	
767	...	−0.31	4.157	...	4.6	177	1	...	...	
768	...	−0.67	4.218	...	5.5	144	1	...	...	
774	...	−0.67	4.24	...	5.7	151	2	...	...	
778	...	−0.58	4.274	...	6.1	84	2	...	...	
782	2267	−0.19	4.19	B5 V	4.8	154	1	0.49	2.776	
783	...	0.01	4.137	...	4.3	117	1	...	...	
792	2350	−0.23	4.24	...	5.4	222	2	0.451	2.733	
814	...	−0.07	4.114	...	4.1	219	...	...	...	
853	...	−0.34	4.201	...	5.1	101	1	...	...	
854	...	−0.26	4.171	...	4.7	155	1	...	...	
859	...	−0.5	4.191	...	5	198	1	...	...	
862	...	−0.17	4.175	...	4.7	90	1	...	...	
870	...	−0.09	4.158	...	4.5	377	1	...	...	
878	...	−0.22	4.171	...	4.7	282	1	...	...	Δv = −43
884	...	−0.13	4.172	...	4.6	235	1	...	...	
892	...	−0.16	4.161	...	4.6	183	1	...	...	
893	...	−0.28	4.166	...	4.7	253	1	...	...	Δv = −38
896	804	−0.1	4.156	...	4.5	301	1	0.538	2.644	
903	...	−0.19	4.192	...	4.9	59	1	...	...	
918	2111	−0.14	4.169	...	4.6	173	1	0.567	2.724	
920	...	−0.19	4.177	...	4.7	81	1	...	...	
939	...	0	4.154	...	4.4	306	1	...	...	
940	...	0	4.161	...	4.5	167	1	...	...	
941	...	0.14	4.157	...	4.4	134	1	...	...	
942	...	−0.33	4.203	...	5.1	222	1	...	...	
952	2116	−0.12	4.163	B8 V	4.6	116	1	0.593	2.71	
954	830	−0.25	4.27	B3 V	5.8	224	2	...	...	
970	784	−0.02	4.168	B8 V	4.6	228	1	0.596	2.565	
973	...	−0.19	4.176	...	4.7	170	1	...	...	
986	...	0.09	4.147	...	4.3	322	1	...	...	
1007	...	−0.23	4.175	...	4.7	319	1	...	...	Δv = −41:
1009	...	0.05	4.171	...	4.5	327	1	...	...	
1017	...	0.18	4.125	...	4.1	189	1	...	...	

TABLE 1—*Continued*

ID (1)	Oosterhoff (2)	M_V (3)	Log ($T_{\rm eff}$) (4)	Spectral Type (5)	Mass ($M_\odot$) (6)	$v \sin i$ (km s^{-1}) (7)	Group (8)	c_0 (9)	β (10)	Binarity (11)
1018	...	−0.05	4.152	...	4.4	80	1	...	...	$\Delta v = -37$:
1040	...	0.08	4.153	...	4.4	272	1	...	...	
1053	...	−0.01	4.171	...	4.6	356	1	...	...	$\Delta v = 76$
1102	...	0.18	4.132	...	4.2	257	1	...	...	
1124	...	0.22	4.131	...	4.1	249	1	...	...	
1128	2426	0.28	4.129	B8 V	4.1	261	1	...	...	$\Delta v = 32$
1140	...	0.08	4.149	...	4.3	249	1	...	...	
1141	...	−0.11	4.223	...	5.1	272	1	...	...	
1169	...	0.35	4.156	...	4.2	55	1	...	...	
1170	...	0.2	4.137	...	4.2	251	1	...	...	
1172	1077	0.11	4.136	...	4.2	129	1	0.675	2.781	
1176	...	0.01	4.192	...	4.8	41	1	...	...	
1216	...	0.24	4.133	...	4.1	228	1	...	...	$\Delta v = -44$:
1218	...	0.05	4.17	...	4.5	371	1	...	...	
1234	1049	0.05	4.172	...	4.5	152	1	0.558	2.715	
1250	...	0.18	4.138	...	4.2	234	1	...	...	
1271	...	0.29	4.121	...	4	100	1	...	...	
1280	...	0.16	4.155	...	4.3	21	1	...	...	
1294	...	0.36	4.154	...	4.2	135	1	...	...	
1403	...	0.41	4.142	...	4.1	227	1	...	...	
1405	1118	0.32	4.128	...	4	183	1	0.721	2.833	
1518	...	0.41	4.152	...	4.2	21	1	...	...	$\Delta v = 50$

The resulting spectra were extracted, cosmic-ray–cleaned, combined, and wavelength-calibrated using standard DOHYDRA IRAF reduction scripts. The resulting values of the signal-to-noise ratio (S/N) ranged from 25 to 100 per resolution element for a typical target.

We also obtained spectra of 25 B1–B9 stars in the I Lac association; 18 of these stars, with spectral types in the range B1–B3, have published projected rotational velocities spanning the range 20–365 km s^{-1} (Abt & Hunter 1962) and served as standards.

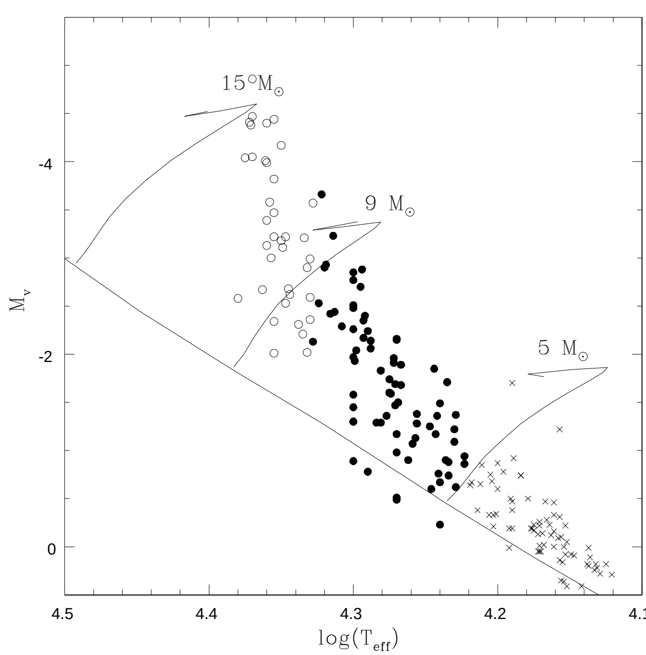

Fig. 1.—The M_V vs. log $T_{\rm eff}$ diagram for the stars in h and χ Per. The data are from SHM02. For analysis, these stars have been divided according to $T_{\rm eff}$ into three groups, represented from hottest to coolest by the open circles, filled circles, and crosses, respectively. Also shown are the ZAMS and evolutionary tracks for models representing stars with masses of 15, 9, and 5 $M_\odot$ from Schaller et al. (1992).

2.2. *Derived Rotational Velocities*

Rotational velocities for the hotter stars in our sample (stars in the two higher temperature groups shown in Fig. 1) were determined (1) by establishing the relationship between the FWHM for He I and Mg II and projected rotational velocity ($v \sin i$) for the I Lac rotational standard stars and (2) using this relationship and the measured FWHM to establish $v \sin i$ for the unknowns (following Abt et al. 2002, hereafter ALG02). FWHM was determined from a Gaussian fit to the observed profiles. For the stars in these two groups, the He I line is substantially stronger than the Mg II line and was given twice the weight in deriving the average $v \sin i$ from the two lines. The relationships between FWHM and $v \sin i$ for the standard stars are shown in Figure 2, which demonstrates a good correlation between line width and $v \sin i$.

Several stars in our h and χ Per sample that fall in our two higher temperature groups have also been observed by Gies & Huang (2004; 2004, private communication). These authors derive values of $v \sin i$ by fitting three He I lines ($\lambda\lambda$4026, 4387, 4471) with profiles derived from model atmospheres. Their computed profiles take limb and gravity darkening into account. Figure 3 shows a comparison between the values of $v \sin i$ derived by Gies & Huang and those in the current study. The best-fitting straight line is given by

$$v \sin i\,(\text{Gies \& Huang}) = 1.05(\pm 0.06)\, v \sin i\,(\text{current study}) + 11(\pm 9)\ \text{km s}^{-1}. \quad (1)$$

Our results thus correlate well with the measurements of Gies & Huang but are systematically smaller by about 5%. Gies & Huang in turn state that their calibration agrees with the

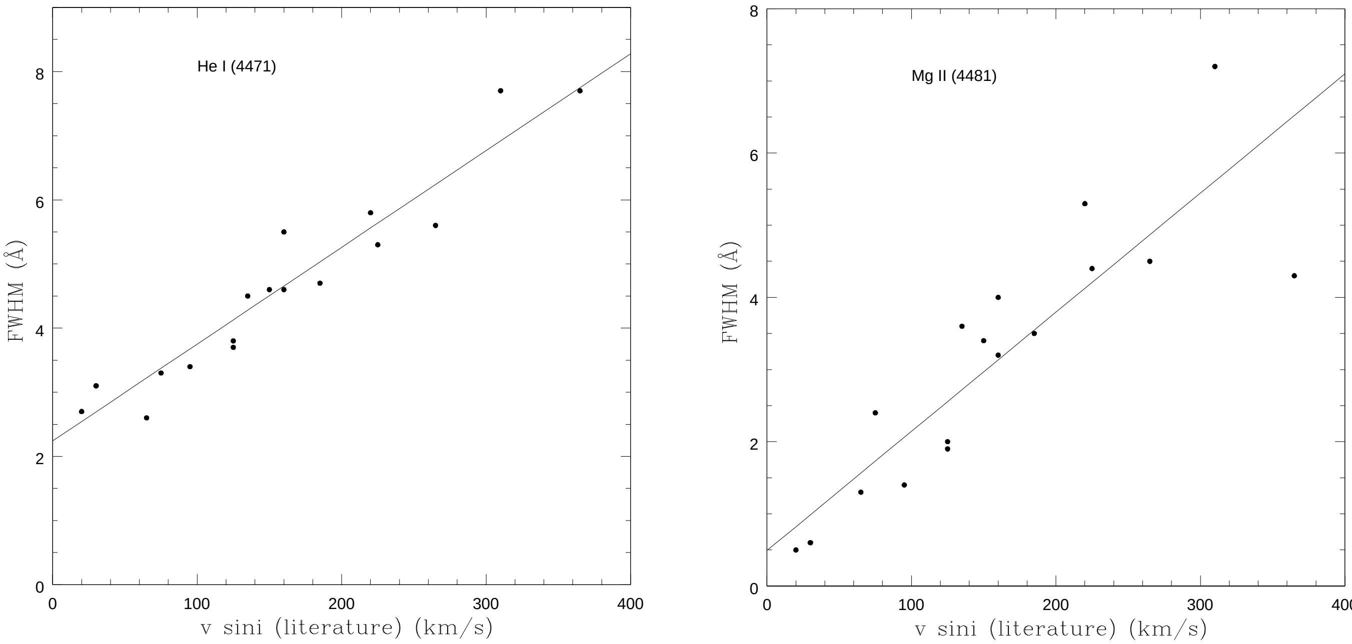

FIG. 2.—Relationships between the FWHMs of He I λ4471 (*left*) and Mg II λ4481 (*right*) and $v \sin i$ for standard stars in I Lac (Abt & Hunter 1962). The best least-squares fit to the data is shown in each panel.

calibrations of Slettebak (1968, 1985) with a best-fit slope of 0.999 and a zero-point offset of 34 km s^{-1} in the sense that the Gies & Huang measurements are smaller than the Slettebak values. We have 13 stars in common with Slettebak and find that $v \sin i\,(\text{Slettebak}) = 1.13\, v \sin i\,(\text{current study}) + 39$ km s^{-1}, again indicating that our results are systematically slightly smaller. The Slettebak measurements were made from photographic plates with dispersions of 40 and 47 Å mm^{-1} and were insensitive to rotations less than about 50 km s^{-1}, which likely accounts for the zero-point offset.

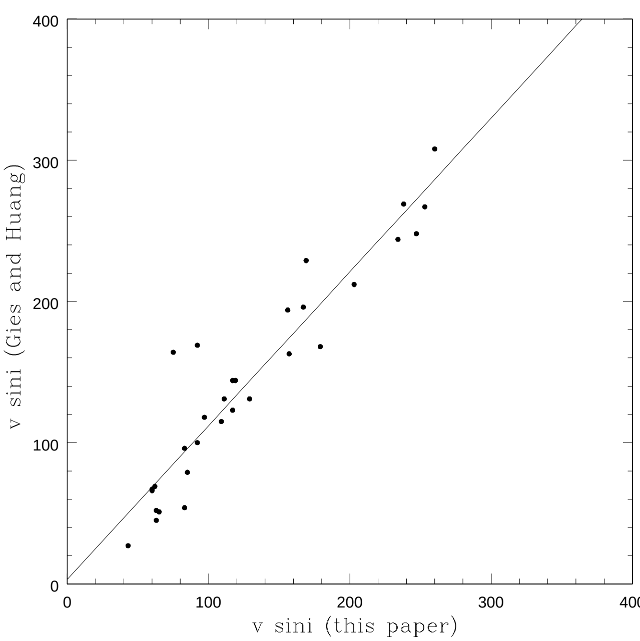

FIG. 3.—Comparison between the values of $v \sin i$ measured in the current study and those derived by D. R. Gies & W. Huang (2004, private communication) for stars in h and χ Per that are common to the two programs. The best-fitting straight line is given by $v \sin i\,(\text{Gies \& Huang}) = 1.05\, v \sin i\,(\text{current study}) + 11$ km s^{-1}.

To calibrate the rotational velocities for stars in the coolest temperature group, we made use of a previous set of Hydra observations of stars with low rotational velocities measured by ALG02 and having spectral types in the range B0–B8 (HR 1855, B0 V, $v \sin i = 10$ km s^{-1}; HR 2222, B1 V, $v \sin i = 0$ km s^{-1}; HR 153, B2 IV, $v \sin i = 10$ km s^{-1}; HR 6042, B5 V, $v \sin i = 30$ km s^{-1}; and HR 677, B8 V, 25 km s^{-1}). We artificially broadened these spectra by convolving the observed standard star spectra with a rotational broadening profile corresponding to projected velocities of 50, 100, 150, 200, 300, 350, and 400 km s^{-1}. Over this entire spectral range, we find that the FWHMs of the calculated broadened line profiles are well correlated with rotation speed and that the slope and zero point of the relationships for the 4471 and 4481 Å lines do not vary significantly with spectral type. Guided by this result, we chose to adopt the ($v \sin i$, FWHM) relationships derived empirically for the two hotter groups for the cooler group as well. Because the He I and Mg II lines have similar equivalent widths for stars in the coolest group, the two lines were given equal weight in deriving $v \sin i$.

Line widths become relatively insensitive to rotation once the rotation rate approaches the critical velocity because of the effects of gravity darkening. Townsend et al. (2004) have constructed models of rapidly rotating B stars and find that for B0–B7 stars viewed equator-on and rotating at 95% of the critical velocity, the measured velocity will be up to 17% too low for measurements of Mg II λ4481 and up to 33% too low for measurements of He I λ4471 if gravity darkening is ignored. The effects are much smaller both for lower rotation rates and smaller angles of inclination. For stars in our sample, critical velocities range from about 400 to more than 500 km s^{-1}. We find that $N(v \sin i)$, the distribution of apparent $v \sin i$, decreases rapidly with increasing rotation above 250 km s^{-1}. Only about 12% of the h and χ Per stars in the two lowest mass bins, and fewer than 5% of the field stars, appear to rotate faster than 300 km s^{-1} (see Fig. 6). Hence, the fraction of our sample that might be strongly affected by gravity darkening is insignificant ($<10\%$).

The values of $v \sin i$ derived from the FWHMs are listed in column (7) of Table 1. Where more than one observation of a star is available, the quoted $v \sin i$ value represents an average of all determinations. The internal accuracy of our $v \sin i$ determinations can be assessed by comparing estimates derived from independent observations obtained on different nights. From such a comparison, we conclude that our reported $v \sin i$ values have an internal uncertainty of ~10%. From the comparisons with the data of Gies & Huang (2004) and of Slettebak (1968) for h and χ Per, we have shown that the data transform to an externally calibrated system with a systematic uncertainty of about 5%–10%.

2.3. *Radial Velocities and the Search for Binaries*

A number of studies (e.g., Abt & Hunter 1962; ALG02) suggest possible correlations between binarity and observed rotational velocity. We have two methods for detecting binaries with our data set: (1) we can identify those spectra that have double lines and (2) we can look for stars with radial velocities that differ significantly from the cluster mean. For each star in our sample, we have derived a radial velocity from the observed line centroid wavelengths of the He I and Mg II lines.

The internal accuracy of the velocity determinations was judged by comparing the mean velocity derived from the He I and Mg II lines for three individual 1800 s exposures that when summed constituted the 120 minute observation of one of the faint fields. Because the pairs of exposures are separated by no more than 45 minutes, we expect any intrinsic radial velocity variations over this short time to be negligible compared with measurement errors. This comparison should give us a worst-case estimate of the errors, since the S/N of the observations of the faint stars is somewhat lower than for the bright stars and because (as we show in § 4) the rotation rates of the fainter stars are somewhat higher and broader lines are harder to measure.

In Figure 4, we depict the cumulative distribution of velocity differences for one pair of exposures for the fainter stars in our sample. Note that about 85% of the stars have velocity differences that are less than 10 km s^{-1}. Only about 3% of the stars have velocity differences greater than 30 km s^{-1}, and the fact that a few stars have large errors is a consequence of the difficulty of measuring centroids of very broad lines.

This result provides the basis for compiling a list of candidate spectroscopic binaries. To be considered a candidate binary, the average velocity of a star on the summed exposures had to differ from the mean cluster velocity derived from the full sample of 216 stars by 30 km s^{-1}. In addition, a few stars showed double lines. Column (11) of Table 1 indicates which stars are candidate spectroscopic binaries and the reason for their candidacy. For double-lined stars, the velocity listed is the difference in the velocities of the two components. For single-lined stars, the table gives the difference between the stellar velocity and the cluster mean. The velocities marked with a colon are based on a single line. For the bright stars, the velocity difference listed in column (11) is based on data from a single night. For only two of the bright stars was there a significant difference with the velocity measured on a second night. Star 33 shows a change in velocity of 200 km s^{-1}, which confirms its binary nature. Star 150 shows a velocity difference of 34 km s^{-1}, just barely significant given our criteria. This star may also be a binary but has not been so designated in Table 1. We note finally, that our criterion for selecting candidate spectroscopic binaries could result in missing objects with velocity differences relative to the cluster mean close to 30 km s^{-1} in cases in which the rotation speed of the primary exceeds 300 km s^{-1}. However, as noted previously, such rapidly rotating objects comprise less than 10% of our field and cluster samples.

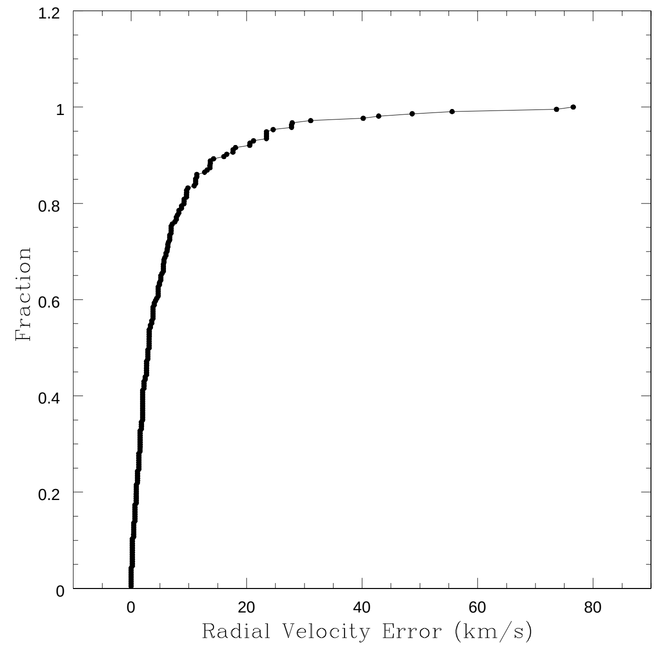

Fig. 4.—Cumulative distribution of velocity differences between pairs of exposures of the same stars taken less than 45 minutes apart. Since radial velocity should not change significantly over this short interval of time, the differences can be taken as an estimate of the measurement error. Note that only about 3% of the stars have velocity differences greater than 30 km s^{-1}.

3. THE COMPARISON SAMPLE: FIELD B STARS

The B stars in h and χ Per are members of high stellar density, bound systems. Isolated field B stars of ages comparable to that of h and χ Per (~12 Myr) are most likely drawn from stars born in much lower density environments: (1) stars formed initially in isolation or in small aggregates or (2) stars whose peculiar motions have carried them several tens of parsecs away from their birthplaces in loose OB associations. The population of isolated field B stars may also contain a small number of stars born in dense environments but later ejected via gravitational encounters (runaway stars).

Extensive observations of rotational velocities for bright field B stars are available in the literature. The recent study by ALG02 provides a homogeneous database for a large (1092 stars) sample of field B stars listed in the Bright Star Catalog. Their observations were obtained with a CCD and have a resolution of 0.11 Å or 7.1 km s^{-1}. The rotational velocities quoted by ALG02 were calibrated against Slettebak et al. (1975) standards. Since D. R. Gies & W. Huang (2004, private communication) have shown that their data for h and χ Per are consistent with this system and our measurements are about 5% smaller than the Gies & Huang values, a comparison between our h and χ Per data and the ALG02 data should be valid to within the externally calibrated uncertainties of ~5%–10%. We note that while the ALG02 sample, drawn from the Bright Star Catalog, is dominated by isolated field stars, it contains as well a very modest number of stars located in relatively dense environments (e.g., the Orion Nebula Cluster). We have not attempted to exclude such stars from the sample, but note that including them will tend to reduce any differences between the distribution of rotational velocities between our h and χ Per and field samples.

The surface rotation rates of stars can be expected to change as stars evolve because of the changing moment of inertia of the star, transport of angular momentum within the star, and possible loss of angular momentum due to winds. Hence, in order to assess intrinsic differences in the distribution of rotation speeds among stars in h and χ Per and the field, it is essential that the field star sample include only objects having ages comparable to h and χ Per (12–15 Myr; see Fig. 1 and SHM02). To do this requires luminosity and effective temperature values of precision sufficient to enable age estimates. Because most stars in the ALG02 catalog lack parallaxes accurate enough to derive luminosities relative to the zero-age main sequence (ZAMS) and thus stellar age, we have established their evolutionary state by using the Strömgren β and c_0 indices. These indices provide accurate estimates of surface gravity and effective temperature, respectively, thus allowing evaluation of stellar ages: the youngest stars will have the highest surface gravities for fixed effective temperature (large β index at constant c_0), whereas more evolved stars will have lower surface gravities and thus smaller β indices.

In order to select field stars of ages comparable to those of the h and χ Per sample, we made use of the Strömgren β and c_1 indices listed by Hauck & Mermilliod (1998) for the ALG02 sample. For h and χ Per, values of β and c_1 are available from measurements reported by Crawford et al. (1970) and by Capilla & Fabregat (2002). Apropos photometry of the ALG02 sample, Hauck & Mermilliod (1998) have carefully transformed heterogeneous data from the literature to the Crawford system, noted discrepant values, and given them low weight. For h and χ Per, Capilla & Fabregat (2002) have used as standard stars objects in clusters measured by Crawford and collaborators or objects measured by other investigators who made use of the same photometer-telescope combinations as Crawford. We thus believe that the Strömgren photometry for both the ALG02 field stars and the h and χ Per sample has been transformed carefully to the Crawford system and can thus be intercompared with confidence.

For the field stars, we used the relationship between intrinsic color ($B-V$) and spectral type (Drilling & Landolt 2000) to estimate the reddening and calculate the reddening-corrected Strömgren index, c_0. For those few stars for which values of $B-V$ were not available from the Simbad database, we have assumed zero reddening. Given that the reddening $E(c_1)$ for the B stars for which we do have color information is typically 0.01–0.02 mag and seldom exceeds 0.03 mag, any uncertainties in the reddening are unimportant for the analysis in this paper. The c_1 indices observed for the h and χ Per sample have been transformed to c_0 by assuming an average reddening of $E(b-y) = 0.4$ [i.e., $E(c_1) = 0.2E(b-y)$; see Capilla & Fabregat 2002]. The relationships between β and M_V and c_0 and $T_{\rm eff}$ coupled with the group boundaries shown in Figure 1 were then used to establish boundaries between groups 1, 2, and 3 in the (β, c_0) plane. The subset of the ALG02 sample falling within these boundaries is plotted in Figure 5; the symbols indicate those stars in the ALG02 sample that correspond to groups 1, 2, and 3. Also shown in this figure are the location of the subset of stars in the h and χ Per sample for which published Strömgren photometry is available.

Table 2 lists the values of β and c_0 (or c_1, for the stars lacking $B-V$ measurements; see above) for the field stars plotted in Figure 5 along with the values of $v \sin i$ from ALG02 and the assignment of the star to one of the three temperature groups defined for the h and χ Per sample.

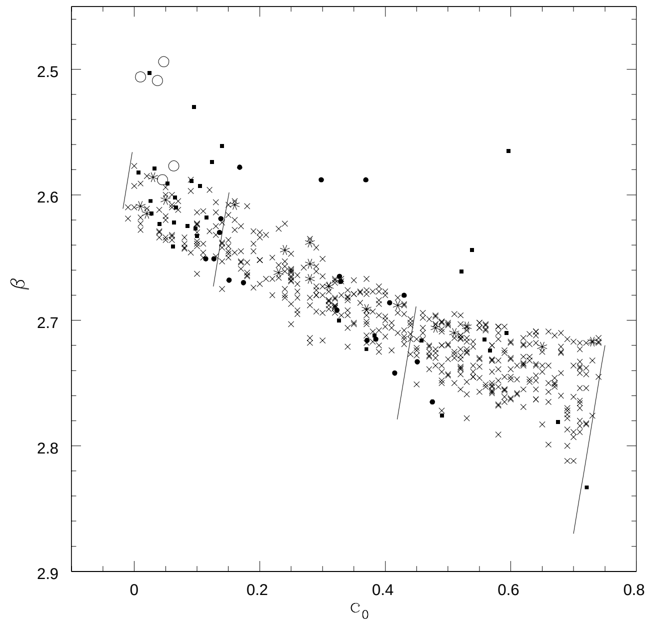

Fig. 5.—Measured values of β and c_0 for ALG02 field stars included in our sample (*crosses*). The boundaries between groups are shown as solid lines. Filled circles and squares represent measurements for that subset of the h and χ Per sample with published photometry; open circles indicate known emission-line objects in h and χ Per (Bragg & Kenyon 2002; Keller et al. 2001). The outliers for the h and χ Per sample may represent either objects having unreported hydrogen line emission, objects rotating at 0.9 times breakup speed but viewed at a modest inclination angle (Collins & Sonneborn 1977), or lower quality measurements.

We note that the field stars in the ALG02 sample that fall within low- (group 1) and intermediate- (group 2) temperature groups comprise not only objects of luminosity class V but of luminosity classes III and even II (although the latter comprise <1% of groups 1 and 2). At first glance, this would appear surprising, given that stars in groups 1 and 2 are expected to be little evolved from their initial location on the ZAMS and thus to have reported spectra consistent with assignment to luminosity class V. However, in the temperature range spanned by these two groups, the actual difference in luminosity between class III and class V is quite modest. Quantitatively, the difference in the (β, c_0) plane between the mean relationships for luminosity classes V and III is 0.04 mag in β, which corresponds to only 0.4 mag in absolute visual magnitude (Crawford 1978). By comparison, the full range of β values at a given c_0 among late B stars nominally assigned to luminosity class V is almost 0.1 mag, thus resulting in significant overlap in β values with stars assigned to luminosity class III. Hence, the appearance of some stars classified as luminosity class III among the objects assigned to groups 1 and 2 on the basis of their location in the (β, c_0) plane is in fact expected. That the range of β values is as large as 0.1 mag for a given spectral type and luminosity class almost certainly reflects both the subjectivity inherent in any visual classification, as well as small errors introduced by assigning discrete spectral types as opposed to a continuously varying indicator of effective temperature, c_0.

Because (β, c_0) photometry provides finer resolution in both temperature and luminosity than MK classification and because we have confidence that the ALG02 and h and χ Per sample have been transformed appropriately to the Crawford system, we believe that using the observed locations of the ALG02 and h and χ Per stars in the (β, c_0) plane provides the most reliable

TABLE 2
DATA FOR FIELD STARS

HR	HD	Spectral Type	$v \sin i$ (km s^{-1})	β	c_0
Group 1					
15.............	358	B8 IVmnp	50	2.743	0.52
28.............	584	B7 IV	15	2.757	0.55
61.............	1256	B6 III/IV	150	2.741	0.49
70.............	1438	B8 V	20	2.751	0.67
78.............	1606	B7 V	104	2.737	0.52
96.............	2054	B9 IV	40	2.775	0.69
121...........	2729	B6 V	95	2.709	0.49
123...........	2772	B8 Vn	220	2.754	0.71
137...........	3038	B9 III	195	2.778	0.69
144...........	3240	B7 III	60	2.75	0.67
149...........	3322	B8 IIImnp	25	2.732	0.58
223...........	4636	B9 III	95	2.739	0.58
326...........	6676	B8 V	120	2.742	0.71
345...........	6972	B9 IV	100	2.812	0.70
348...........	7019	B7 III–IV	60	2.741	0.65
364...........	7374	B8 III	25	2.747	0.60
369...........	7546	B9 IIIsp	25	2.719	0.62
438...........	9298	B7 IIImnp	50	2.739	0.60
491...........	10425	B8 IIIn	240	2.715	0.69
561...........	11857	B5 III	25	2.717	0.54
562...........	11905	B8 III	40	2.71	0.58
612...........	12767	B9.5sp	45	2.714	0.51
677...........	14272	B8 V	25	2.763	0.64
682...........	14392	B9sp	90	2.772	0.49
702...........	14951	B7 IV	215	2.727	0.51
746...........	16004	B9mnp	30	2.753	0.56
760...........	16219	B5 V	30	2.72	0.49
785...........	16727	B7 IIIp	20	2.729	0.47
811...........	17081	B7 IV	25	2.717	0.60
836...........	17543	B6 V	70	2.703	0.48
846...........	17743	B8 III	50	2.741	0.57
847...........	17769	B7 V	145	2.741	0.54
873...........	18296	B9p	25	2.767	0.58
890...........	18537	B7 V	90	2.739	0.52
896...........	18604	B6 III	105	2.72	0.57
910...........	18883	B7 V	65	2.758	0.57
954...........	19832	B6 IV–V	110	2.746	0.55
982...........	20315	B8 V	185	2.736	0.65
1038..........	21364	B9 Vn	195	2.783	0.65
1047..........	21455	B7 V	120	2.731	0.55
1051..........	21551	B8 V	295	2.746	0.67
1094..........	22316	B9p	150	2.778	0.53
1097..........	22402	B8 Vn	320	2.731	0.60
1100..........	22470	B8/B9 III	128	2.728	0.47
1113..........	22780	B7 Vne	230	2.705	0.53
1140..........	23288	B7 IV	185	2.749	0.63
1141..........	23300	B6 V	20	2.702	0.49
1144..........	23324	B8 V	185	2.748	0.64
1145..........	23338	B6 IV	105	2.702	0.55
1146..........	23363	B7 V	140	2.735	0.64
1172..........	23753	B8 V	290	2.737	0.71
1202..........	24388	B8 V	135	2.736	0.61
1207..........	24504	B6 V	130	2.721	0.47
1213..........	24587	B5 V	30	2.744	0.50
1243..........	25330	B5 V	140	2.724	0.45
1305..........	26670	B5 Vn	270	2.715	0.46
1307..........	26676	B8 Vn	175	2.748	0.58
1315..........	26793	B9 Vn	275	2.732	0.73
1328..........	27026	B9 V	220	2.783	0.72
1363..........	27563	B5 III	35	2.703	0.52
1375..........	27742	B8 IV–V	175	2.763	0.64
1377..........	27777	B8 V	250	2.744	0.64

TABLE 2—*Continued*

HR	HD	Spectral Type	$v \sin i$ (km s^{-1})	β	c_0
1397..........	28114	B6 IV	25	2.698	0.46
1399..........	28149	B7 V	115	2.726	0.48
1402..........	28217	B8 IV	60	2.717	0.53
1424..........	28503	B8 V	60	2.73	0.55
1445..........	28929	B9p	55	2.749	0.53
1449..........	29009	B9sp	55	2.701	0.49
1469..........	29335	B7 V	65	2.75	0.51
1484..........	29589	B8 IV	70	2.728	0.45
1576..........	31373	B9 V	70	2.731	0.52
1600..........	31764	B7 V	140	2.71	0.68
1610..........	32040	B9 Vn	295	2.77	0.69
1671..........	33224	B8 V	155	2.755	0.64
1696..........	33802	B8 V	185	2.755	0.59
1705..........	33949	B7 V	120	2.717	0.70
1750..........	34762	B9 IV	230	2.743	0.72
1757..........	34863	B7–B8 V	285	2.734	0.62
1759..........	34880	B8 III	45	2.724	0.59
1769..........	35104	B8 II	95	2.725	0.47
1791..........	35497	B7 III	60	2.703	0.56
1860..........	36589	B6 V	90	2.728	0.52
1902..........	37098	B9 IV–V	50	2.768	0.58
1920..........	37320	B8 III	25	2.736	0.64
1945..........	37646	B8 IV	130	2.762	0.60
1957..........	37808	B9.5 IIIsp	30	2.722	0.45
1985..........	38478	B8 IIImnp	55	2.705	0.58
1997..........	38670	B9 Vn	215	2.745	0.59
2038..........	39417	B9 V	145	2.75	0.66
2109..........	40574	B8 IIIn	205	2.709	0.64
2116..........	40724	B8 V	130	2.776	0.73
2127..........	40964	B8 V	115	2.782	0.72
2130..........	41040	B8 III	140	2.718	0.60
2139..........	41269	B9sp	85	2.766	0.71
2202..........	42657	B9mnp	65	2.737	0.55
2207..........	42784	B8 Vnn	370	2.72	0.57
2223..........	43153	B7 V	65	2.756	0.57
2237..........	43362	B9 III	145	2.77	0.71
2248..........	43526	B7 III	75	2.696	0.52
2297..........	44766	B8 IIIn	170	2.745	0.60
2374..........	46075	B6 III	50	2.736	0.62
2438..........	47395	B7 III	65	2.714	0.53
2454..........	47756	B8 IIIs	30	2.715	0.58
2461..........	47964	B8 III	45	2.718	0.72
2497..........	49028	B8 IV	45	2.72	0.49
2519..........	49606	B7 III	20	2.702	0.50
2521..........	49643	B8 IIIn	255	2.723	0.52
2522..........	49662	B7 IV	90	2.751	0.45
2589..........	51104	B8 Vn	160	2.753	0.67
2605..........	51688	B8 III	35	2.705	0.53
2613..........	51892	B7 III	50	2.704	0.56
2676..........	53929	B9.5 III	25	2.708	0.53
2760..........	56446	B8 III	185	2.725	0.65
2826..........	58346	B8/B9 V	165	2.754	0.72
2860..........	59136	B5 III	65	2.712	0.64
2922..........	60863	B8 V	185	2.756	0.59
2947..........	61554	B6 V	280	2.712	0.52
2949..........	61556	B5 IVn	70	2.75	0.57
2956..........	61672	B7 V	280	2.726	0.59
3201..........	68099	B6 III	50	2.72	0.62
3353..........	71997	B4 V	15	2.72	0.47
3470..........	74604	B8 V	150	2.759	0.61
3500..........	75333	B9mnp	35	2.747	0.63
3607..........	77665	B8 V	90	2.738	0.72
3652..........	79158	B8 IIImnp	60	2.706	0.55
3982..........	87901	B7 V	300	2.723	0.71
4119..........	90994	B6 V	80	2.73	0.48

TABLE 2—*Continued*

HR	HD	Spectral Type	$v \sin i$ (km s^{-1})	β	c_0
4493..........	101391	B9p	50	2.765	0.59
4696..........	107348	B8 V	195	2.738	0.71
4857..........	111226	B8 V	70	2.73	0.60
4967..........	114376	B7 III	115	2.712	0.52
5250..........	121847	B8 V	165	2.757	0.66
5407..........	126769	B8 V	195	2.753	0.57
5475..........	129174	B9p	25	2.745	0.54
5597..........	133029	B9sp	30	2.8	0.69
5614..........	133529	B7 V	310	2.732	0.57
5655..........	134946	B8 III	150	2.738	0.52
5733..........	137391	F0 V	90	2.745	0.74
5780..........	138764	B6 IV	20	2.72	0.50
5910..........	142250	B6 Vp	15	2.75	0.49
6003..........	144844	B9 V	20	2.791	0.58
6023..........	145389	B9mnp	20	2.787	0.69
6054..........	146001	B8 V	90	2.748	0.49
6079..........	146926	B8 V	180	2.736	0.70
6294..........	152909	B7–B8 III	50	2.752	0.57
6340..........	154204	B7 IV–V	275	2.725	0.51
6520..........	158704	B9 II–III	20	2.757	0.57
6545..........	159376	Ap	164	2.726	0.68
6567..........	159975	B8 II–IIImnp	95	2.718	0.74
6720..........	164447	B8 Vne	170	2.721	0.65
6919..........	169990	B8 III–IV	110	2.764	0.71
6967..........	171247	B8 IIIsp	55	2.717	0.73
6968..........	171301	B8 IV	40	2.772	0.69
6990..........	171961	B8 III	55	2.721	0.54
6997..........	172044	B8 II–IIIp	30	2.696	0.48
7035..........	173117	B8 III	30	2.705	0.58
7039..........	173300	B8 III	35	2.733	0.71
7073..........	173936	B6 V	90	2.739	0.47
7113..........	174933	B9 II–IIIp	20	2.753	0.58
7115..........	174959	B6 IV	50	2.707	0.49
7147..........	175744	B9sp	50	2.701	0.49
7239..........	177817	B7 V	130	2.742	0.68
7241..........	177863	B8 V	60	2.731	0.57
7245..........	178065	B9 III	15	2.718	0.71
7248..........	178125	B8 III	60	2.755	0.59
7283..........	179527	B9sp	35	2.712	0.67
7285..........	179588	B9 IV	35	2.812	0.69
7339..........	181558	B5 III	20	2.715	0.44
7346..........	181828	B9 V	145	2.747	0.61
7358..........	182255	B6 III	25	2.736	0.48
7361..........	182308	B9mnp	15	2.699	0.47
7395..........	183056	B9sp	35	2.714	0.52
7401..........	183339	B8 IVwe	45	2.706	0.48
7437..........	184606	B8 IIIn	185	2.709	0.64
7447..........	184930	B5 III	55	2.707	0.56
7452..........	184961	B9sp	40	2.789	0.70
7457..........	185037	B8 Vne	315	2.717	0.73
7466..........	185268	B5 V	195	2.694	0.46
7493..........	186122	B9 III	20	2.729	0.63
7543..........	187235	B8 Vn	315	2.76	0.68
7593..........	188293	B7 Vn	190	2.73	0.51
7607..........	188651	B6 V+	150	2.715	0.52
7608..........	188665	B5 V	105	2.715	0.45
7642..........	189432	B5 IV	15	2.723	0.48
7664..........	190229	B9mnp	20	2.695	0.51
7721..........	192276	B7 V	25	2.745	0.54
7737..........	192659	B9 IV–V	20	2.769	0.62
7786..........	193722	B9sp	35	2.711	0.63
7814..........	194636	B4 V	30	2.763	0.60
7840..........	195483	B8 V	140	2.759	0.53
7852..........	195810	B6 III	50	2.702	0.55
7878..........	196426	B8 IIIp	20	2.735	0.62

TABLE 2—*Continued*

HR	HD	Spectral Type	$v \sin i$ (km s^{-1})	β	c_0
7885..........	196606	B8 IIIn	50	2.729	0.62
7922..........	197226	B6 III	90	2.736	0.54
7961..........	198174	B7 IIIp	65	2.705	0.59
7963..........	198183	B5 Ve	100	2.71	0.51
7978..........	198513	B8np	175	2.761	0.70
8022..........	199578	B5 V	30	2.71	0.46
8033..........	199728	Ap	55	2.732	0.63
8065..........	200614	B8 III	20	2.714	0.74
8094..........	201433	B9 V	25	2.789	0.71
8106..........	201834	B9 III	25	2.732	0.57
8109..........	201888	B7 III	5	2.725	0.53
8118..........	202149	B9mnp	35	2.78	0.71
8141..........	202753	B5 V	20	2.703	0.48
8158..........	203206	B6 IV	60	2.755	0.52
8161..........	203245	B6 V	75	2.731	0.50
8218..........	204428	B6 V	125	2.726	0.53
8226..........	204754	B8 III	20	2.709	0.66
8240..........	205087	B9sp	30	2.799	0.66
8292..........	206540	B5 IV	20	2.719	0.50
8338..........	207516	B8 V	95	2.784	0.71
8348..........	207840	B8 III	15	2.755	0.62
8349..........	207857	B9mnp	20	2.704	0.50
8355..........	208008	B9 V	45	2.743	0.50
8377..........	208727	B8 V	205	2.758	0.61
8403..........	209419	B5 III	20	2.697	0.48
8418..........	209819	B8 V	135	2.793	0.70
8452..........	210424	B5 III	20	2.723	0.53
8478..........	210934	B8 III	50	2.736	0.66
8512..........	211838	B8 IIImnp	65	2.721	0.68
8554..........	212986	B5 III	30	2.736	0.49
8705..........	216523	B8 V	30	2.761	0.59
8706..........	216538	B7 III–IV	20	2.706	0.55
8723..........	216831	B7 III	65	2.714	0.62
8861..........	219749	B9p	65	2.765	0.66
8873..........	219927	B8 III	15	2.718	0.64
8887..........	220222	B6 III	115	2.708	0.56
8902..........	220575	B8 III	20	2.717	0.74
9031..........	223640	Ap	30	2.751	0.56
9086..........	224906	B9 IIImnp	35	2.725	0.68
9087..........	224926	B7 III–IV	60	2.703	0.50
9091..........	224990	B4 III	15	2.706	0.46
9110..........	225289	B8mnp	40	2.719	0.63
Group 2					
38.............	829	B2 V	0	2.652	0.20
91.............	1976	B5 IV	125	2.693	0.38
155...........	3379	B2.5 IV	55	2.695	0.26
189...........	4142	B5 V	160	2.702	0.41
302...........	6300	B3 V	100	2.68	0.33
801...........	16908	B3 V	90	2.682	0.32
930...........	19268	B5 V	25	2.719	0.43
950...........	19736	B4 V	50	2.677	0.36
987...........	20365	B3 V	120	2.681	0.34
989...........	20418	B5 V	260	2.673	0.39
1005..........	20756	B5 IV	30	2.718	0.37
1011..........	20809	B5 V	185	2.696	0.39
1029..........	21071	B7 V	50	2.727	0.44
1034..........	21278	B5 V	50	2.705	0.40
1044..........	21428	B3 V	125	2.686	0.36
1063..........	21699	B8 IIImnp	35	2.696	0.37
1121..........	22920	B9 IIIsp	30	2.687	0.43
1153..........	23466	B3 V	90	2.688	0.31
1174..........	23793	B3 V	20	2.684	0.34
1194..........	24155	B9sp	35	2.706	0.34
1199..........	24263	B5 V	105	2.711	0.44

TABLE 2—*Continued*

HR	HD	Spectral Type	$v \sin i$ (km s^{-1})	β	c_0
1244..........	25340	B5 V	80	2.708	0.43
1253..........	25558	B3 V	30	2.694	0.32
1258..........	25631	B2.5 V	220	2.654	0.18
1312..........	26739	B5 IV	30	2.677	0.40
1350..........	27396	B4 IV	15	2.678	0.36
1378..........	27778	B3 V	105	2.682	0.34
1415..........	28355	B3 V	0	2.713	0.40
1553..........	30870	B5 V	110	2.701	0.37
1582..........	31512	B6 V	80	2.695	0.43
1617..........	32249	B3 V	30	2.656	0.23
1640..........	32612	B2.5 IV	65	2.665	0.18
1641..........	32630	B3 V	95	2.684	0.31
1719..........	34233	B5 V	35	2.71	0.42
1731..........	34447	B3 IV	10	2.657	0.24
1748..........	34748	B1.5 Vn	295	2.639	0.14
1749..........	34759	B3 V	55	2.717	0.38
1753..........	34798	B5 IV–V	30	2.703	0.37
1765..........	35039	B2 IV–V	5	2.628	0.16
1786..........	35407	B4 IVn	295	2.683	0.32
1798..........	35532	B2 Vn	260	2.623	0.24
1810..........	35708	B2.5 IV	10	2.642	0.14
1820..........	35912	B2 V	5	2.671	0.20
1839..........	36267	B5 V	155	2.724	0.41
1848..........	36430	B2 V	15	2.674	0.19
1851..........	36485	B2 V	35	2.653	0.17
1864..........	36653	B3 V	155	2.685	0.31
1871..........	36741	B2 V	175	2.65	0.15
1875..........	36819	B2.5 IV	105	2.671	0.26
1891..........	37016	B2.5 V	100	2.687	0.25
1898..........	37040	B2.5 IV	145	2.68	0.24
1900..........	37055	B3 IV	50	2.716	0.30
1906..........	37150	B3 Vvar	190	2.653	0.14
1924..........	37367	B2 IV–V	20	2.629	0.19
1928..........	37438	B3 IV	40	2.668	0.25
1946..........	37711	B3 IV	105	2.672	0.31
1951..........	37752	B8p	35	2.697	0.40
2005..........	38804	B5 V	40	2.713	0.43
2128..........	40967	B5 III	45	2.679	0.35
2161..........	41814	B3 V	35	2.718	0.28
2198..........	42545	B5 Vn	245	2.68	0.40
2199..........	42560	B3 IV	160	2.669	0.33
2205..........	42690	B2 V	0	2.634	0.20
2213..........	42927	B3 III	95	2.682	0.26
2224..........	43157	B5 V	30	2.673	0.29
2232..........	43317	B3 IV	130	2.665	0.30
2266..........	43955	B2/B3 V	40	2.661	0.24
2273..........	44112	B2.5 V	95	2.65	0.22
2282..........	44402	B2.5 V	25	2.677	0.26
2292..........	44700	B3 V	0	2.696	0.33
2306..........	44953	B8 III	30	2.691	0.31
2325..........	45321	B2.5 V	160	2.684	0.31
2344..........	45546	B2 V	70	2.652	0.20
2361..........	45813	B4 V	120	2.692	0.37
2380..........	46189	B2.5 V	85	2.673	0.30
2433..........	47247	B3 V	70	2.72	0.39
2490..........	48879	B4 IV	105	2.668	0.35
2494..........	48977	B2.5 V	20	2.669	0.25
2509..........	49333	B7 II–III	65	2.689	0.32
2537..........	50012	B2 IV	70	2.62	0.16
2544..........	50093	B2 III–IV	150	2.632	0.21
2603..........	51630	B2 III–IV	20	2.616	0.15
2611..........	51823	B2.5 V	70	2.676	0.29
2614..........	51925	B2.5 III	165	2.636	0.15
2616..........	52018	B2 V	50	2.666	0.25
2621..........	52140	B3 V	0	2.702	0.35

TABLE 2—*Continued*

HR	HD	Spectral Type	$v \sin i$ (km s^{-1})	β	c_0
2623..........	52273	B2 III	80	2.605	0.16
2625..........	52348	B3 V	145	2.677	0.31
2640..........	52670	B2 V	17	2.635	0.28
2680..........	54031	B3 V	0	2.689	0.32
2688..........	54224	B2 IV–V	10	2.645	0.19
2695..........	54669	B4 V	115	2.645	0.15
2704..........	54912	B2.5 IV	40	2.639	0.19
2718..........	55522	B2 IV–V	95	2.664	0.26
2756..........	56342	B3 V	5	2.676	0.34
2774..........	56876	B2 IV–V	310	2.676	0.37
2799..........	57573	B2.5 V	190	2.667	0.33
2800..........	57593	B2.5 V	105	2.659	0.25
2824..........	58325	B2 IV–V	5	2.645	0.17
2921..........	60855	B2–B3 V	240	2.609	0.18
2948..........	61555	B6 V	107	2.714	0.28
3192..........	67797	B5 IV	140	2.684	0.39
3194..........	67880	B2.5 V	15	2.63	0.20
3454..........	74280	B3 V	95	2.653	0.24
3849..........	83754	B5 V	150	2.7	0.40
4456..........	100600	B4 V	140	2.688	0.32
5191..........	120315	B3 V	150	2.694	0.30
5764..........	138485	B2 Vn	210	2.654	0.17
5902..........	142096	B2.5 V	155	2.703	0.25
5904..........	142114	B2.5 Vn	250	2.68	0.22
5907..........	142184	B2 V	280	2.662	0.25
5912..........	142301	B8 III–IV	90	2.693	0.29
5915..........	142378	B2–B3 V	225	2.69	0.32
5928..........	142669	B2 IV–V	120	2.647	0.15
5942..........	142990	B5 IV	125	2.682	0.24
5985..........	144218	B2 V	65	2.675	0.14
5988..........	144334	B8 V	55	2.721	0.34
5998..........	144661	B8 IV–V	45	2.708	0.39
6042..........	145792	B6 IV	30	2.725	0.39
6092..........	147394	B5 IV	30	2.702	0.44
6141..........	148605	B2 V	175	2.662	0.18
6502..........	158148	B5 V	240	2.688	0.43
6588..........	160762	B3 IV	0	2.661	0.29
6692..........	163685	B3 IV	10	2.679	0.37
6741..........	164900	B3 Vn	260	2.67	0.32
6851..........	168199	B5 V	175	2.687	0.39
6873..........	168797	B3 Ve	260	2.644	0.24
6924..........	170111	B3 V	120	2.692	0.34
6946..........	170740	B2 V	25	2.641	0.15
6984..........	171780	B5 Vne	230	2.688	0.42
7033..........	173087	B5 V	85	2.712	0.37
7081..........	174179	B3 IVpsh	5	2.657	0.29
7100..........	174585	B3 IV	145	2.66	0.25
7121..........	175191	B2.5 V	165	2.667	0.21
7166..........	176162	B5 IV	200	2.703	0.35
7179..........	176502	B3 V	0	2.667	0.32
7185..........	176582	B5 IV	65	2.692	0.26
7210..........	177003	B2.5 IV	10	2.675	0.24
7258..........	178329	B3 V	0	2.69	0.32
7306..........	180554	B4 IV	80	2.677	0.39
7347..........	181858	B3 IVp	0	2.696	0.34
7355..........	182180	B2 Vn	320	2.666	0.23
7372..........	182568	B3 IV	100	2.667	0.22
7374..........	182618	B5 V	35	2.706	0.41
7467..........	185330	B5 II–III	15	2.667	0.37
7565..........	187811	B2.5 Ve	195	2.667	0.28
7647..........	189687	B3 IVe	230	2.638	0.28
7651..........	189775	B5 III	85	2.668	0.32
7656..........	189944	B4 V	10	2.704	0.44
7700..........	191263	B3 V	60	2.68	0.30
7739..........	192685	B3 V	160	2.658	0.27

TABLE 2—*Continued*

HR	HD	Spectral Type	$v \sin i$ (km s^{-1})	β	c_0
7862	196035	B3 IV	20	2.688	0.28
7870	196178	B9sp	50	2.709	0.38
7899	196775	B3 V	210	2.665	0.25
7911	197018	B6 IIImnp	55	2.699	0.44
7912	197036	B5 IV	135	2.679	0.35
7927	197419	B2 IV–Ve	105	2.655	0.28
7929	197511	B2 V	35	2.651	0.30
7996	198820	B3 III	15	2.677	0.38
8029	199661	B2.5 IV	130	2.682	0.28
8064	200595	B3 Vn	285	2.682	0.42
8136	202654	B4 IV	160	2.68	0.29
8301	206672	B3 IV	55	2.642	0.29
8341	207563	B2 V	85	2.647	0.25
8356	208057	B3 Ve	110	2.673	0.31
8439	210191	B2.5 IV	10	2.627	0.23
8520	212076	B2 IV–Ve	80	2.608	0.16
8528	212222	B5 V	35	2.715	0.43
8535	212454	B8 III–IV	40	2.694	0.42
8549	212883	B2 V	5	2.659	0.17
8553	212978	B2 V	120	2.646	0.16
8579	213420	B2 IV	70	2.625	0.17
8758	217543	B3 Vpesh	305	2.662	0.23
8768	217811	B2 V	0	2.661	0.25
8770	217833	B9 IIIwe	30	2.691	0.37
8777	217943	B2 V	145	2.664	0.18
9011	223229	B3 IV	30	2.68	0.29
		Group 3			
39	886	B2 IV	0	2.629	0.12
153	3360	B2 IV	10	2.625	0.13
779	16582	B2 IV	5	2.624	0.10
1072	21803	B2 IV	40	2.61	0.06
1191	24131	B1 V	95	2.623	0.01
1215	24640	B1.5 V	150	2.646	0.09
1463	29248	B2 III	20	2.612	0.07
1552	30836	B2 III+	35	2.606	0.13
1595	31726	B1 V	5	2.634	0.05
1679	33328	B2 IVne	325	2.604	0.05
1770	35149	B1 V	220	2.617	0.05
1781	35299	B1.5 V	0	2.636	0.05
1783	35337	B2 IV	15	2.632	0.06
1790	35468	B2 III	55	2.613	0.11
1833	36166	B2 V	125	2.641	0.10
1840	36285	B2 IV–V	15	2.646	0.11
1842	36351	B1.5 V	20	2.639	0.11
1855	36512	B0 V	10	2.597	0.09
1861	36591	B1 IV	5	2.61	−0.01
1873	36779	B2.5 V	175	2.649	0.13
1886	36959	B1 Vvar	5	2.629	0.04
1887	36960	B0.5 V	20	2.6	0.05
1892	37018	B1 V	20	2.619	−0.01
1896	37023	B0.5 Vp	80	2.61	0.00
1911	37209	B1 V	35	2.63	0.04
1913	37232	B2 IV–V	110	2.642	0.08
1918	37303	B1 Vvar	265	2.618	0.01
1923	37356	B2 IV–V	10	2.623	0.10
1932	37479	B2 VpHe	165	2.586	0.03
1933	37481	B1.5 IV	90	2.636	0.06
1950	37744	B1.5 V	25	2.634	0.04
2031	39291	B2 IV–V	150	2.639	0.10
2058	39777	B1.5 V	20	2.65	0.11
2294	44743	B1 II–III	17	2.593	0.00
2373	46064	B2 III	60	2.638	0.14
2387	46328	B1 III	0	2.585	0.02
2618	52089	B2 Iab:	25	2.577	0.00
2628	52437	B3 Vnn	190	2.622	0.14
2648	52918	B1 V	270	2.591	0.01
2733	55856	B2 IV	40	2.614	0.10
2734	55857	B0.5 V	150	2.605	0.07
2739	55879	B0 III	30	2.588	0.09
2743	55985	B2 IV–V	30	2.632	0.13
2928	61068	B2 III	10	2.62	0.05
3004	62747	B1.5 III	95	2.6	0.06
3023	63271	B2 IV–V	30	2.643	0.08
5885	141637	B1.5 Vn	225	2.637	0.10
6453	157056	B2 IV	30	2.623	0.10
6601	161056	B1.5 V	235	2.594	0.05
6684	163472	B2 IV–V	75	2.63	0.10
6719	164432	B2 IV	50	2.614	0.13
6787	166182	B2 IV	30	2.608	0.15
7335	181409	B2 IVe	140	2.615	0.02
7940	197770	B2 III	55	2.596	0.12
8007	199140	B2 III	45	2.611	0.02
8238	205021	B1 IV	20	2.628	0.01
8603	214167	B2 Ve	265	2.609	0.01
8640	214993	B2 III	30	2.612	0.04
8651	215191	B1 V	180	2.633	0.06
8725	216916	B2 IV	10	2.639	0.08
8733	217101	B2 IV–V	130	2.663	0.10
9005	223128	B2 IV	10	2.634	0.08
9071	224572	B1 V	150	2.608	0.06

means of sorting each sample into identical temperature and age groups.

Could the use of photometric indices as opposed to spectroscopic sorting introduce any subtle selection biases? One concern is that rapid rotation may alter observed β and c_0 indices sufficiently to either exclude rapidly rotating stars from the sample or to move them across the boundaries defining our three temperature groups. Empirical (Crawford 1978) and theoretical (Collins & Sonneborn 1977) studies suggest that changes in β and c_0, driven by temperature and gravity variations as a function of latitude among rotationally distorted stellar surfaces, are in practice significant only for stars having rotation speeds in excess of 250 km s^{-1}. The most rapidly rotating stars among the cohort with rotation speeds in excess of 250 km s^{-1} may exhibit Hβ emission, the presence of which could change measured β sufficiently to drive the star outside the bins used to define our groups. However, examination of the ALG02 sample suggest that only 8%, 6%, and 3% of stars in the temperature range spanned by groups 1, 2, and 3, respectively, have rotation speeds higher than 250 km s^{-1}. These percentages represent strong upper limits on the actual fraction of stars that would either be excluded from our sample completely or moved from one group to another. Consequently, we believe that selection via location in the (β, c_0) plane will not produce significant biases in the derived distributions of rotation speeds.

For the purpose of assessing whether the frequency of close binaries has an effect on the comparison of rotational velocities of the h and χ Per sample with stars in the field, we have searched the Ninth Spectroscopic Binary Catalog[2] for orbital

[2] See http://sb9.astro.ulb.ac.be.

TABLE 3
DATA FOR FIELD STAR BINARIES

HR	HD	Spectral Type	$v \sin i$ (km s^{-1})	β	c_0	K (km s^{-1})
Group 1						
354	7157	B9 V	22	2.789	0.632	ALG:sb2
936	19356	B8 V	50	2.748	0.616	sb2:44
1033	21203	B9 V+. . .	50	2.791	0.684	ALG:sb2
1088	22203	B9 V	65	2.765	0.702	sb2:103
1185	23950	B8 III	60	2.746	0.607	ALG:sb2
1240	25267	B6 V+. . .	30	2.733	0.611	sb1:41
1347	27376	B9 V	20	2.768	0.63	sb2:64
1471	29365	B8 V	70	2.757	0.601	sb1:65
1690	33647	B9 Vn	30	2.771	0.687	ALG:sb2
1847	36408	B7 IIIe	45	2.711	0.706	ALG:sb2
2226	43179	B7 V	25	2.763	0.616	ALG:sb2
2784	57103	B8 V	55	2.774	0.648	sb2:106
3623	78316	B8 IIImnp	15	2.717	0.558	sb1:67
5801	139160	B7 IV	25	2.74	0.451	sb1:37
5863	140873	B8 III	80	2.744	0.499	sb2:43
5906	142165	B5 V	220	2.74	0.481	sb1:33
6620	161701	B9 V	25	2.754	0.641	sb1:52
6928	170200	B8 III–IV	40	2.745	0.631	sb1:38
7109	174853	B8 Vnn	100	2.763	0.636	ALG:sb2
7171	176301	B7 III–IV	75	2.707	0.593	ALG:sb2
7174	176318	B7 IV	120	2.75	0.579	sb1:76
7326	181182	B8 III+	60	2.725	0.603	sb2:70
8036	199892	B7 III	20	2.731	0.535	sb1:43
8357	208095	B6 IV–V	95	2.747	0.508	sb2:106
8567	213236	B8 II	15	2.737	0.669	ALG:sb2
Group 2						
154	3369	B5 V	25	2.688	0.433	sb2:48
226	4727	B5 V	20	2.71	0.407	sb2:72
1163	23625	B2.5 V	20	2.654	0.146	sb2:82
1239	25204	B3 V+. . .	50	2.691	0.352	sb2:57
1288	26326	B4 V	5	2.69	0.391	ALG:sb2
1420	28475	B5 V	30	2.711	0.432	sb2:80
1497	29763	B3 V	115	2.713	0.356	sb2:54
1659	32990	B2 V	55	2.64	0.241	sb1:37
1764	35007	B3 V	35	2.691	0.277	ALG:sb2
1803	35588	B2.5 V	170	2.663	0.189	sb1:71
1863	36646	B4 Vn	180	2.69	0.271	ALG:sb2
1890	37017	B1.5 V	165	2.65	0.136	sb1:36
2052	39698	B2 V	115	2.635	0.185	sb2:70
2159	41753	B3 V	30	2.653	0.317	sb1:33
2598	51411	B3 V	0	2.707	0.376	ALG:sb2
5812	139365	B2.5 V	100	2.689	0.263	sb2:75
5934	142883	B3 V	5	2.721	0.317	sb1:64
6028	145482	B2 V	165	2.657	0.177	sb1:32
6414	156247	B5 Vnn	110	2.695	0.390	sb2:180
6431	156633	B1.5 V	140	2.648	0.206	sb2:98
6621	161756	B4 IVe	95	2.665	0.349	ALG:sb2
6738	164852	B3 IV	150	2.685	0.295	sb2:58
6773	165814	B4 IV	200	2.674	0.389	sb2:151
7131	175426	B2.5 V	110	2.666	0.303	sb1:40
7305	180553	B8 V	70	2.704	0.362	sb1:55
7486	185936	B5 V	65	2.704	0.426	sb1:47
7688	190993	B3 V	115	2.686	0.293	ALG:sb2
7777	193536	B2 V	80	2.63	0.219	sb2:115
7861	195986	B4 III	0	2.672	0.385	sb1:32
8001	199081	B5 V	40	2.713	0.397	sb2:112
8384	208947	B2 V	125	2.654	0.188	sb2:116
8397	209288	B5 IIIn	75	2.7	0.390	ALG:sb2
8427	209961	B2 V	145	2.638	0.167	sb1:122
8606	214240	B3 V	55	2.678	0.374	sb1:82
8800	218407	B2 V	100	2.639	0.165	sb1:86
8803	218440	B2 V	25	2.664	0.166	sb2:88
8808	218537	B3 V	80	2.695	0.255	ALG:sb2
8926	221253	B3 IV	140	2.681	0.295	sb1:57

TABLE 3—*Continued*

HR	HD	Spectral Type	$v \sin i$ (km s^{-1})	β	c_0	K (km s^{-1})
Group 3						
1131......................	23180	. . .	100	2.597	0.022	sb2:112
1333......................	27192	B1.5 IV	110	2.604	0.027	ALG:sb2
1567......................	31237	B3 III+	90	2.603	0.135	sb1:58
1811......................	35715	B2 IV	110	2.622	0.027	sb2:139
1868......................	36695	B1 V	120	2.625	0.012	sb2:129
1894......................	37021	B0 V	240	2.602	0.125	sb2:66
1952......................	37756	B2 IV–V	75	2.632	0.111	sb2:89
4590......................	104337	B1.5 V	95	2.607	0.078	sb2:120
5056......................	116658	B1 III–IV	130	2.607	0.018	sb2:120
5944......................	143018	B1 V	90	2.614	0.016	sb2:124
5984......................	144217	B1 V	100	2.615	−0.017	sb2:125
7200......................	176819	B2 IV–V	40	2.640	0.095	sb1:55

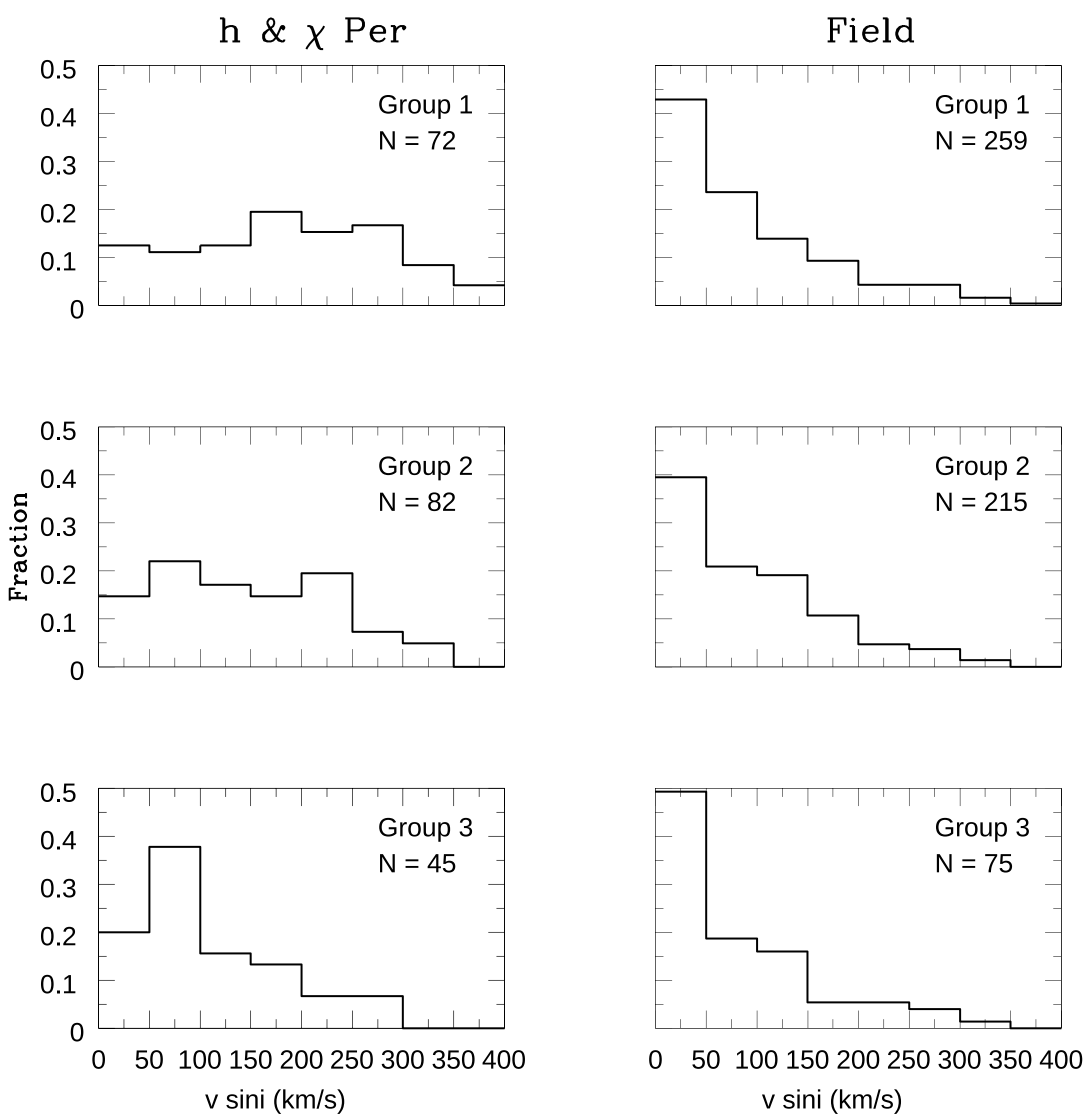

FIG. 6.—Distribution of $v \sin i$ for each of the three groups of stars in h and χ Per compared with the distributions for field stars. Note the large differences in the distributions for the stars in the coolest group (group 1) and the progressive convergence of the distributions with increasing temperature.

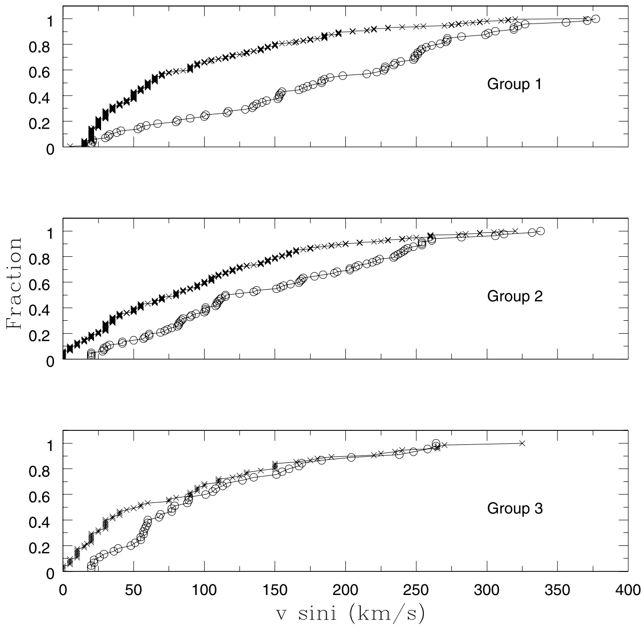

FIG. 7.—Cumulative distribution of $v \sin i$ for the stars in h and χ Per (*open circles*) compared with the distributions for field stars (*crosses*) of similar temperature and age. Stars of group 1 comprise late B stars, little evolved from the ZAMS. Stars of group 2 comprise middle B stars, evolved from the ZAMS by less than 1.0 mag. Stars of group 3 comprise early B stars, significantly evolved from the ZAMS. In all cases, the fraction of stars with $v \sin i < 100$ km s^{-1} is larger in h and χ Per, with the largest difference occurring for group 1, i.e., for late B stars.

parameters for stars in the ALG02 sample. In h and χ Per, we can detect binaries only if they differ from the cluster mean velocity by more than 30 km s^{-1} or if we see double lines. Therefore, in Table 3, we list those field stars that (1) meet our color criteria, (2) have orbital semiamplitudes greater than 30 km s^{-1}, and/or (3) for which ALG02 reported seeing double lines. The last column of Table 3 indicates whether each star is a single-lined binary (sb1) or doubled-lined (sb2) and gives the amplitude of the velocity variation, which was taken from the Ninth Spectroscopic Binary Catalog. ALG:sb2 indicates that the only evidence for binarity is the report of double lines in ALG02. We recognize that the colors of spectroscopic binaries do not provide an accurate reflection of the temperature and surface gravity of the primary star, but we cannot make corrections for this effect for either h and χ Per or the field stars and so treat both samples identically.

4. DISTRIBUTION OF ROTATIONAL VELOCITIES

In Figure 6, we plot the frequency distributions of rotational velocity $N(v \sin i)$ for each of the three groups we have defined. All of the stars in our samples are included in the plots; these include the spectroscopic binary candidates identified in h and χ Per, as well as the primaries of binaries in the field star sample. We have excluded the secondaries in the field star sample because in most cases we lack the temperature data needed to assign them to one of our three groups. In Figure 7, we plot the cumulative distributions for the $v \sin i$ data shown in Figure 6. These figures suggest that the $N(v \sin i)$ distribution for the h and χ Per group 1 stars (those that are little evolved from the ZAMS) is strikingly different from that of the field stars of similar mass and age. The distribution of $v \sin i$ for the middle group of stars in h and χ Per also differs from that of the field stars in the same temperature range, but the difference is smaller. The distributions

TABLE 4
AVERAGE VALUES OF $v \sin i$

Definition of Sample	$\langle v \sin i \rangle$ (km s^{-1})	No. of Stars
Group 1:		
All stars...		
h and χ Per members	183	72
Field stars	92	259
Binaries $K > 30$ km s^{-1} excluded...		
h and χ Per members	184	62
Field stars	96	234
Binaries $K > 30$ km s^{-1} only...		
h and χ Per Members	183	10
Field stars	56	25
Group 2:		
All stars...		
h and χ Per members	145	82
Field stars	93	215
Binaries $K > 30$ km s^{-1} excluded...		
h and χ Per members	156	73
Field stars	95	177
Binaries $K > 30$ km s^{-1} only...		
h and χ Per Members	44	9
Field stars	84	38
Group 3:		
All stars...		
h and χ Per members	104	45
Field stars	83	75
Binaries $K > 30$ km s^{-1} excluded...		
h and χ Per members	104	42
Field stars	79	63
Binaries $K > 30$ km s^{-1} only...		
h and χ Per members	100	3
Field stars	108	12

of $v \sin i$ for evolved stars in the hottest group (group 3) exhibit only a small difference.

In all three temperature ranges, the sense of the difference is the same: while the number of rapid rotators ($v \sin i > 250$ km s^{-1}) and the maximum rotation velocity measured are similar for both field and cluster stars, there is a marked deficiency of slow rotators ($v \sin i < 100$ km s^{-1}) among the cluster stars. In order to assess the statistical significance of these differences, we calculated the corresponding K-S probabilities that the distributions are drawn from the same distribution. These probabilities are 2×10^{-10}, 9×10^{-6}, and 9×10^{-3} for groups 1, 2, and 3, respectively.

Table 4 summarizes the average rotational velocities $\langle v \sin i \rangle$ for the stars in h and χ Per and the field. If we consider all of the stars in the sample, including binaries, we find that for the unevolved stars in the coolest temperature region (group 1), the mean $v \sin i$ in h and χ Per is twice that of their field counterparts and that the distributions are different with a high degree of significance. For stars in the middle temperature range, the $\langle v \sin i \rangle$ in h and χ Per is 1.56 times that of the field, and the distributions are different, with a lower, but still high, degree of significance. For the evolved stars in group 3, the $\langle v \sin i \rangle$ in h and χ Per is only 1.25 times that of the field, and the distributions differ, but only marginally.

As a check on the robustness of our result, we computed mean values of $v \sin i$ for the field stars using published spectral types and luminosity classes as opposed to Strömgren photometry. For the purposes of this test, the temperature boundaries for groups 1, 2, and 3 were defined to be B5–B9, B2.5–B5, and B0–B2, respectively. Stars with luminosity classes III–V were included. The resulting mean values are 112, 109, and 113 km s^{-1}, respectively, for groups 1, 2, and 3. Although these values differ by 15%–20% from those listed in Table 4, our basic conclusions regarding the differences between the h and χ Per and field samples remain the same: the rotation speeds for groups 1 and 2 are significantly higher in h and χ Per as compared with the field, whereas for group 3, the rotation speeds between cluster and field are indistinguishable statistically.

The number of detectable spectroscopic binaries in h and χ Per is insufficient to enable comparison of the *distribution* of rotational velocities for the binaries among the three separate groups at a high level of statistical significance. Instead, we have calculated the mean rotational speeds, $\langle v \sin i \rangle$, for the binaries in each of the groups. We note that assignments to each of the groups are based on observed colors, which reflect the luminosity-weighted contributions from the primary and secondary components. For all binaries the effective temperature of the primary assigned on the basis of color will thus be smaller than its true effective temperature.

The values of $\langle v \sin i \rangle$ for the binaries with $K > 30$ km s^{-1} and for the complementary samples excluding the binaries are compared in Table 4. For group 1, the field binaries have a $\langle v \sin i \rangle$ value only 58% as large as $\langle v \sin i \rangle$ for the field stars not in known binaries with $K > 30$ km s^{-1}. For groups 2 and 3, the differences in $\langle v \sin i \rangle$ between the binaries with $K > 30$ km s^{-1} and the remaining stars in the same temperature range are not significant. Because only ~10% of the stars show evidence of radial velocity variations greater than 30 km s^{-1}, we conclude that the distributions of rotation speeds for h and χ Per and the field presented above are not affected significantly by the inclusion or exclusion of binaries from the sample.

5. DISCUSSION

Our results show that relatively unevolved stars in h and χ Per (those in group 1 that presumably reflect their initial angular momenta most accurately) rotate on average more rapidly than stars of comparable age in the field by about a factor of 2. The stars with larger masses in groups 2 and 3 also rotate more rapidly than field stars with similar masses and evolutionary states, but the differences decrease with increasing mass. The differences in mean rotation speed between h and χ Per and the field stars primarily reflect a paucity of slowly rotating stars in the double cluster, particularly among stars in groups 1 and 2. It has been known for a long time (e.g., Slettebak 1968) that there are a large number of Be stars in h and χ Per, so the fact that we find a bias toward rapidly rotating stars in these clusters is perhaps not surprising. We note as well that the observed distribution of rotation speeds in h and χ Per is unusual compared with other, albeit lower density, clusters (e.g., Brown & Verschueren 1997).

What causes the differences in $N(v \sin i)$ between h and χ Per and the field? Is the near absence of slow rotation seen in h and χ Per a consequence of a difference in the initial conditions that characterize the formation of stars in a dense, bound cluster as compared with the presumably lower density regions in which field stars form? If so, what specific differences in initial conditions are the determining factors? Why do the distributions of $v \sin i$ for h and χ Per stars appear to converge progressively toward the distributions of $v \sin i$ seen for the field stars in the two hotter regions? Is this apparent convergence the result of processes that are effective after stars reach the ZAMS? Or was the similarity of $N(v \sin i)$ between h and χ Per and the field found for early B stars imposed at the time of star formation?

5.1. *Rotation Changes during Evolution away from the ZAMS*

We consider first the question of how evolution affects $N(v \sin i)$ after stars reach the ZAMS and specifically whether it is plausible that the massive stars in group 3 initially shared the high average rotation speeds of their cooler, lower mass cohorts in groups 1 and 2 but converged to the field star average as they evolved.

Heger & Langer (2000) and Meynet & Maeder (2000) have calculated models of evolving rotating stars for stars spanning the masses represented among group 3. These models show that qualitatively, as high-mass main-sequence stars evolve from the ZAMS toward the end of core hydrogen burning, their surface rotation should decrease as a result of (1) changes in stellar moments of inertia and (2) loss of stellar angular momentum via strong stellar winds. However, the magnitude of the decrease in surface rotation rate is predicted to be modest because the loss of angular momentum from the surface layers is partially compensated by the transport of angular momentum from the core of the star. For a 12 $M_\odot$ star, Heger & Langer predict that the rotation rates of stars initially rotating at 300 km s^{-1} or less will decline by only 20%–25% during the course of their main-sequence lifetimes; surface rotation begins to increase only after core hydrogen is exhausted and stars approach the terminal-age main sequence (TAMS). Stars of this mass whose initial rotation speeds exceed 300 km s^{-1} are predicted to slow by an additional 10% during the first ~2 Myr after they reach the ZAMS.

Similarly, for a 9 $M_\odot$ star rotating initially at 300 km s^{-1}, Meynet & Maeder predict a 27% decrease in $v \sin i$ during main-sequence evolution. Since the decrease of rotation speed as the star evolves from the ZAMS to a point just prior to the TAMS is predicted to be nearly identical in percentage terms for stars of differing initial masses and rotation rates (20%–30% over the range mass range 9–12 $M_\odot$), one might expect some convergence of $\langle v \sin i \rangle$ for two groups of stars, one of which initially contained a large number of rapid rotators and a second group of stars dominated by slow rotators. However, the convergence predicted from extant models (~25%) is much smaller than that required to reduce the mean $v \sin i$ by a factor of 2, the amount required to evolve a distribution of $N(v \sin i)$ from one similar to that observed for stars in group 1 to one closely resembling that found for group 3.

Observations also argue against a factor of 2 decrease in rotation rates as stars evolve. Wolff & Preston (1978) and WEP82 searched for a correlation between $v \sin i$ and age by sorting field B stars according to the Strömgren β index, which through its sensitivity to surface gravity provides a measure of distance from the ZAMS and hence of age. Although this technique is somewhat uncertain, since the β index can be affected both by emission and by extremely rapid rotation, these authors found no significant systematic differences in $\langle v \sin i \rangle$ as a function of distance from the ZAMS and hence argued that any change in $v \sin i$ with age must be small at least for this heterogeneous sample. Abt (2003) looked for systematic differences in $\langle v \sin i \rangle$ between B dwarfs and giants of the same masses among a sample of field stars. By using spectral type as a surrogate for mass, Abt reports that for stars of 9 $M_\odot$ (the highest mass included in his study) rotation rates decline by only 11% from class V to class III stars. Perhaps the best extant evaluation of age-driven rotation changes is that of Gies & Huang (2004), who observed B0–B3 stars (the spectral-type range populating our group 3) in clusters with ages in the range 3–18 Myr. They found evidence for a possible decrease in rotation of about 20% from the ZAMS to ages $t \sim 10$ Myr, followed

TABLE 5
BINARY FREQUENCY: $K > 30$ km s^{-1}

Definition of Sample (1)	Total No. of Stars (2)	No. of Binaries (3)	Binary Fraction (4)
Group 1:			
Field	259	25	0.1
Binary fraction detected in single observation			0.06
h and χ Per detected binaries	71	9	0.13
Group 2:			
Field stars	215	38	0.18
Binary fraction detected in single observation			0.12
h and χ Per detected binaries	79	6	0.08
Group 3:			
Field stars	75	12	0.16
Binary fraction detected in single observation			0.13
h and χ Per detected binaries	45	3	0.07
Total sample:			
Field stars	549	75	0.14
Binary fraction detected in single observation			0.09
h and χ Per detected binaries	195	18	0.09

by an apparent spin-up of perhaps 30% among stars older than 10 Myr; this spin-up occurs well before the stars reach the TAMS and is not predicted by the models of single rotating stars.

Both theoretical calculations and observations therefore argue against the hypothesis that the early B stars in h and χ Per initially rotated twice as rapidly as their counterparts in the field. Rather, it appears that the differences between h and χ Per and the field stars are intrinsically largest among the late B stars and diminish with increasing mass.

Several authors over the years have reported results similar to those that we find here—namely, that stars in clusters rotate more rapidly than stars in the field (e.g., Bernacca & Perinotto 1974; WEP82; Gies & Huang 2004; Keller 2004). In the latter two cases, the difference was attributed to evolutionary effects. Gies & Huang suggested that the field stars might represent a population that is somewhat older than their sample of fairly young cluster stars and that spin-down processes reduce the average rotation rates of the field stars (as predicted by theory). By contrast, Keller, who reports observations of rotation speeds among LMC clusters with ages greater than 10 Myr, suggests that the higher rotation speeds observed among cluster stars results from LMC clusters having ages systematically larger than their field counterparts. In this case, the spin-up among the putatively older LMC cluster sample is attributed to the increase in $\langle v \sin i \rangle$ expected as stars approach the TAMS.

Both studies selected their samples based primarily on spectral type; as a consequence, the age distributions among the field and cluster samples are not well defined. In the current study, we have been careful to match the ages represented among our field and cluster stars, and in any case we find the largest differences between the field and h and χ Per samples among the late-B stars, which are essentially unevolved. Therefore, for the current sample, we cannot attribute the differences in $N(v \sin i)$ to a systematic difference in age between the cluster stars in h and χ Per and the field stars.

5.2. *Initial Conditions and Rotation*

The above results suggest that the effects of evolution on observed $v \sin i$ distributions should in principle be small. Hence, the observed differences between h and χ Per and the field seem most logically attributed to differences in initial conditions. Three different types of initial conditions have been cited as factors that influence the observed angular momentum of stars: (1) binary frequency, (2) composition, and (3) environment.

5.2.1. *Binary Characteristics*

Binary frequency has the potential to influence the rotation of the component stars in two ways. First, closely spaced binaries are expected to have their rotational and orbital motions synchronized. Second, the formation of a binary system, whatever its spacing, may result in a system in which most of the angular momentum resides in orbital motions rather than stellar rotation.

ALG02 examined the issue of synchronization in their sample of field B stars. They conclude that stars with orbital periods of less than 2.4 days rotate synchronously and that stars with periods between 2.4 and 5 days are synchronized within a factor of 2. Moreover, they find that the average rotation observed among stars in close binaries is indeed lower than for apparently single stars, a result expected if orbital and rotational speeds are synchronized. (Note that for a period of 2.4 days, the corresponding rotational velocity of a typical B star would be 60 km s^{-1}.) However, ALG02 warn that the apparent difference in rotation speeds between binary and single stars might also reflect the fact that stars with published orbits are biased toward sharp-lined stars. For their sample of cluster stars, Gies & Huang (2004) also find a difference in the same sense: $\langle v \sin i \rangle = 125$ km s^{-1} for stars known to have variable velocities and 168 km s^{-1} for constant stars.

In order to attribute the more rapid rotation seen among the h and χ Per sample to a difference in the effect of synchronization, h and χ Per would have to be deficient in close binaries. The data presented in Table 1 provide an estimate of the number of stars in our h and χ Per sample with instantaneous observed amplitudes $K > 30$ km s^{-1} based on a comparison of (typically) a single observed radial velocity with the cluster mean. We can use the complete orbital information for the field binaries to estimate what fraction of the field stars would be detected as binaries in a single observation by calculating for each star for which an orbit is known the fraction of time that the observed velocity differs from the average by more than 30 km s^{-1}. Since stars with amplitudes greater than 30 km s^{-1} are all fairly close binaries, we have made the simplifying assumption that their orbits are circular. Column (4) of Table 5 shows the fraction of the field stars either with known orbits and velocity amplitudes $K > 30$ km s^{-1} or that ALG02 reported to have double lines. This fraction refers to the number of binary systems; that is, we have counted each binary pair as one system. Column (4) of this table also shows the fraction of binaries with known orbits that would have been detected with a single observation to have a velocity that differed by more than 30 km s^{-1} from the center-of-mass velocity. This number is to be compared with the fraction in h and χ Per. Given the small number statistics for the h and χ Per sample, there is no evidence for a significant difference in the number of short-period binaries between h and χ Per and the field.

As an additional check on our conclusion that a deficiency of close binaries in h and χ Per is not the explanation for their higher mean rotation speeds, we can ask how $\langle v \sin i \rangle$ for the field stars would change if the field sample contained no close binaries. Reference to Table 5 shows that the fraction of large-amplitude ($K > 30$ km s^{-1}), and therefore close, binaries among the field stars in our three mass intervals ranges from 10% to 18%. If we calculate $\langle v \sin i \rangle$ for the total sample including binaries and the sample excluding those stars with velocity variations greater than 30 km s^{-1}, the two averages for each of the three mass intervals differ by no more than 6% (see Table 4). Based on our analysis of the field star sample, we therefore conclude that even if h and χ Per contained no close binaries, the difference in average rotation speeds between cluster and field samples cannot be explained.

Although the difference in rotation speeds between h and χ Per and field stars cannot be explained by a difference in the fraction of synchronized (close) binaries, recent work by Brown & Verschueren (1997) suggests that the overall frequency of binaries could influence the distribution of $v \sin i$. These authors conclude that the binary stars in the loose Sco OB2 association rotate on average more slowly than single stars. However, most of the detected binaries in this survey are so widely separated that one would not expect synchronization to be effective. Brown & Verschueren suggest instead that the observed slow rotation among the Sco OB2 binaries is a result of preferential allocation of angular momentum to orbital motion rather than stellar rotation during the star formation process. It could be that in a dense region such as h and χ Per, the formation of widely separated binaries is somehow inhibited by dynamical interactions and as a result there is a deficiency of widely separated binaries relative to what is seen in the field. Although such an effect could explain the more rapid rotation seen in h and χ Per, there is at present no way of testing this hypothesis.

5.2.2. *Chemical Composition*

Studies of rotation among B stars in the Magellanic Clouds have led to the suggestion that stars formed in the lower metallicity LMC and SMC rotate more rapidly than stars formed in the solar neighborhood. Indirect evidence cited in support of this hypothesis is the observed anticorrelation between the frequency of Be stars, which are rapid rotators, and metallicity (Maeder et al. 1999). More recently, Keller (2004) has obtained rotational velocities for (1) B0–B2 stars in LMC clusters that have ages between 10 and 30 Myr and (2) LMC field stars in the same range of spectral types. He concluded that both the LMC field and cluster samples rotate more rapidly than their field star counterparts in the Milky Way; the difference is significant at the 2 σ level.

Differing abundances cannot, however, account for the fact that h and χ Per stars on average rotate more rapidly than Galactic field stars. Vrancken et al. (2000) find that the abundances measured for early B giants in h and χ Per are in reasonable agreement with abundances measured by other authors for main-sequence B stars, including nearby field stars.

5.2.3. *Possible Relationship between Initial Conditions and ZAMS Rotation Speeds*

Field B stars are generally assumed to have formed in loose clusters, associations, or aggregates that disperse rapidly. Since the h and χ Per clusters are still bound, it is reasonable to assume that the stars comprising these clusters were formed in regions of higher average protostellar densities than those characterizing the birthplace of a typical field B star. For reasons noted in the introduction, theory suggests that time-averaged protostellar accretion rates are likely to be higher in denser regions. If the linkage between initial density and protostellar accretion rate predicted by theory is correct, current models predict higher rotation speeds among the outcome stellar populations formed in dense regions.

Suppose that (1) material from a protostellar core infalls onto a disk, (2) material is transported to a forming star through a circumstellar accretion disk, and (3) the inner region of the accretion disk is linked to the star via stellar magnetospheric field lines as described in the introduction. If so, various formulations of the accretion process (e.g., Johns-Krull & Gafford 2002) predict that, for fixed magnetic field strength, the rotation rate should vary directly as a (positive) power of the accretion rate, since higher accretion rates tend to crush the stellar magnetosphere and drive the disk/magnetosphere corotation radius of the disk closer to the surface of the star. The rotation rate at the birth line, i.e., when the phase of rapid accretion ends, also depends directly on a power of the protostellar radius, which in turn also depends on the accretion rate, with larger accretion rates leading to larger radii along the birth line. The combination of higher initial angular velocity and higher initial radius for higher accretion rates can in principle lead to higher ZAMS rotation speeds following pre–main-sequence contraction from the birth line to the ZAMS. This notional linkage—high protostellar accretion rates, which lead to high angular rotation speeds along the birth line and, finally, high ZAMS rotation speeds—neglects many important effects: probable complex topology of the magnetic field, the localized structures of the accretion columns, and the differential rotation of the disk and the star, which leads to disconnection of the magnetic field that links the two and reduces the spin-down torque (Matt & Pudritz 2004). Nevertheless, by making plausible assumptions regarding stellar accretion rates in low-density star-forming regions, Wolff et al. (2004) demonstrate that it is possible to account for the observed trends in specific angular momentum with mass for stars in the mass range 0.1–10 $M_{\odot}$.

The large difference in rotation speeds between groups 1 and 2 in h and χ Per and their field analogs may find explanation in the sensitivity of the mass-radius relationship along the stellar birth line to accretion rate over the mass range $M \sim 4$–$12\ M_{\odot}$, i.e., the mass range observed among the h and χ Per and field B star sample discussed above. Over this range of stellar masses, models of the accretion process predict (1) that the radius of the forming star when it is deposited on the birth line is larger for larger accretion rates, but (2) perhaps most significantly, that for all accretion rates, the mass-radius relationship exhibits a sharp maximum in radius at a mass somewhere in the range 4–12 $M_{\odot}$. The local maximum in radius reflects the onset of deuterium shell burning, which produces a substantial expansion in the radius of the accreting protostar; the specific range of masses at which D-shell burning sets in and the radius expands depends in turn on the protostellar accretion rate. The potential significance of a local maximum in radius along the birth line for stars having masses somewhere between 4 and 12 $M_{\odot}$ results from the fact that the rotation rates observed when B stars reach the ZAMS depend on the initial rotation rates at the birth line and the spin-up as stars contract from the birth line to the ZAMS.

We speculate that the large difference between h and χ Per stars and the field among groups 1 and 2 reflects a difference in the mass accretion rates characterizing the cluster (high accretion rate) and field birthplaces (low accretion rate) that in turn produces differences in initial radii along the birth line that are largest among stars having masses in the range 4.5–9 $M_{\odot}$. If correct, stars in this mass range should show the largest difference in rotation speeds—a direct result of greater spin-up during contraction toward the ZAMS. At higher masses, the difference in rotation speeds between cluster and field should be smaller, since the initial radii along the birth line are similar or, for those stars where the birth line meets the ZAMS, identical.

6. CONCLUSIONS

Observations of rotational velocities show that B stars in the h and χ Per double cluster rotate on average more rapidly than field stars of the same mass and age. This result, combined with other similar results in the literature, clearly establishes that the rotation rates of B stars *differ significantly* among stars born in different regions. We have argued that the observed differences are *likely* built in at the time the stars were formed and not a consequence of subsequent evolutionary processes. Since h and χ Per are currently bound clusters, it seems reasonable to assume that stars in these clusters were formed in much denser environments than field B stars of comparable age, which have presumably escaped from the loose clusters, associations, or small groups in which they formed. We have identified two possible explanations for the observed differences in rotation speeds, each related to the density at the time of star formation. One hypothesis is essentially untestable with current facilities: that h and χ Per are deficient in wide binaries relative to the field and that when wide binaries are formed, much of the available angular momentum appears as orbital rather than stellar rotational angular momentum. The second possibility is that protostellar accretion is more rapid in higher density regions and that high accretion rates lead to more rapid rotation—a consequence of the hypothesis that "disk locking" accounts for initial stellar angular momenta. This hypothesis is attractive because the effects of differences in accretion rate during the stellar assembly phase are predicted to be particularly dramatic among B stars. For stars in the mass range 4–12 $M_{\odot}$, the initial radius along the stellar birth line reflects the effects of deuterium shell burning, which causes a substantial expansion of the star; the amount of the expansion and the range of stellar masses over which it occurs both increase with increasing accretion rates. The combination of high initial accretion rate with high initial radius followed by contraction from the birth line to the ZAMS can lead to high ZAMS rotation speeds compared with stars of similar mass formed in regions characterized by lower accretion rates.

We emphasize that our results for h and χ Per, while suggestive, do not provide conclusive evidence of a direct relationship between environment and outcome rotational velocities. With the advent of 8 to 10 m telescopes, it should be possible to test the hypothesis that outcome stellar rotation speeds are in fact linked to initial stellar density among stars born in a wide variety of environments by observing a large sample of stars located in young clusters both the in Milky Way and in the Magellanic Clouds. Such observations will provide the basis for establishing robustly both the cosmic dispersion in $N(v \sin i)$ and systematic differences attributable to initial stellar density, chemical composition, or other parameters. For regions of sufficient youth, it may also be possible to search for differences in the location of the birth line. If the predicted correlations between rotation speed, birth line location, and environment can be found, it would be possible for the first time to link the initial conditions under which star formation takes place to outcome observables—a crucial first step toward a predictive theory of star formation.

REFERENCES

Abt, H. A. 2003, ApJ, 582, 420
Abt, H. A., & Hunter, J. H., Jr. 1962, ApJ, 136, 381
Abt, H. A., Levato, H., & Grosso, M. 2002, ApJ, 573, 359 (ALG02)
Bernacca, P. L., & Perinotto, M. 1974, A&A, 33, 443
Bragg, A. E., & Kenyon, S. J. 2002, AJ, 124, 3289
Brown, A. G. A., & Verschueren, W. 1997, A&A, 319, 811
Capilla, G., & Fabregat, J. 2002, A&A, 394, 479
Collins, G. W., & Sonneborn, G. H. 1977, ApJS, 34, 41
Crawford, D. L. 1978, AJ, 83, 48
Crawford, D. L., Glaspey, J. W., & Perry, C. L. 1970, AJ, 75, 822
Drilling, J. S., & Landolt, A. U. 2000, in Allen's Astrophysical Quantities, ed. A. N. Cox (4th ed.; New York: AIP), 381
Elmegreen, B. G., & Shadmehri, M. 2003, MNRAS, 338, 817
Gies, D. R., & Huang, W. 2004, in IAU Symp. 215, Stellar Rotation, ed. A. Maeder & P. Eenens (San Francisco: ASP), 57
Hauck, B., & Mermilliod, M. 1998, A&AS, 129, 431
Heger, A., & Langer, N. 2000, ApJ, 544, 1016
Johns-Krull, C. M., & Gafford, A. D. 2002, ApJ, 573, 685
Keller, S. C. 2004, Publ. Astron. Soc. Australia, 21, 310
Keller, S. C., Grebel, E. K., Miller, G. J., & Yoss, K. M. 2001, AJ, 122, 248
Königl, A. 1991, ApJ, 370, L39
Maeder, A., Grebel, E. K., & Mermilliod, J.-C. 1999, A&A, 346, 459
Massey, P., & Hunter, D. A. 1998, ApJ, 493, 180
Matt, S., & Pudritz, R. E. 2004, ApJ, 607, L43
McKee, C. F., & Tan, J. C. 2003, ApJ, 585, 850
Meynet, G., & Maeder, A. 2000, A&A, 361, 101
Schaller, G., Schaerer, D., Meynet, G., & Maeder, A. 1992, A&AS, 96, 269
Shu, F. H., Najita, J., Ruden, S. P., & Lizano, S. 1994, ApJ, 429, 797
Sirianni, M., Nota, A., Leitherer, C., De Marchi, G., & Clampin, M. 2000, ApJ, 533, 203
Slesnick, C. L., Hillenbrand, L. A., & Massey, P. 2002, ApJ, 576, 880 (SHM02)
Slettebak, A. 1968, ApJ, 154, 933
———. 1985, ApJS, 59, 769
Slettebak, A., Collins, G. W., II, Parkinson, T. D., Boyce, P. B., & White, N. M. 1975, ApJS, 29, 137
Stahler, S. W. 1988, ApJ, 332, 804
Stolte, A., Grebel, E. K., Brandner, W., & Figer, D. F. 2002, A&A, 394, 459
Townsend, R. H. D., Owocki, S. P., & Howarth, I. D. 2004, MNRAS, 350, 189
Vrancken, M., Lennon, D. J., Dufton, P. L., & Lambert, D. L. 2000, A&A, 358, 639
Wolff, S. C., Edwards, S., & Preston, G. W. 1982, ApJ, 252, 322 (WEP82)
Wolff, S. C., & Preston, G. W. 1978, ApJS, 36, 497
Wolff, S. C., Strom, S. E., & Hillenbrand, L. A. 2004, ApJ, 601, 979